Published online 4 April 2023

NAR Genomics and Bioinformatics, 2023, Vol. 5, No. 2 **1**
https://doi.org/10.1093/nargab/lqad033

Chromosome-level, nanopore-only genome and allele-specific DNA methylation of Pallas's cat, *Otocolobus manul*

Nicole Flack [1], Melissa Drown[2], Carrie Walls[3], Jay Pratte[4], Adam McLain[5] and Christopher Faulk [3,*]

[1]Department of Veterinary and Biomedical Sciences, University of Minnesota, Saint Paul, MN 55108, USA, [2]Department of Ecology, Evolution, and Behavior, University of Minnesota, Saint Paul, MN 55108, USA, [3]Department of Animal Science, University of Minnesota, Saint Paul, MN 55108, USA, [4]Bloomington Parks and Recreation, Miller Park Zoo, Bloomington, IL 61701, USA and [5]Department of Biology and Chemistry, SUNY Polytechnic Institute, Utica, NY 13502, USA

Received December 04, 2022; Revised February 10, 2023; Editorial Decision March 13, 2023; Accepted March 17, 2023

ABSTRACT

Pallas's cat, or the manul cat (*Otocolobus manul*), is a small felid native to the grasslands and steppes of central Asia. Population strongholds in Mongolia and China face growing challenges from climate change, habitat fragmentation, poaching, and other sources. These threats, combined with *O. manul*'s zoo collection popularity and value in evolutionary biology, necessitate improvement of species genomic resources. We used standalone nanopore sequencing to assemble a 2.5 Gb, 61-contig nuclear assembly and 17097 bp mitogenome for *O. manul*. The primary nuclear assembly had 56× sequencing coverage, a contig N50 of 118 Mb, and a 94.7% BUSCO completeness score for *Carnivora*-specific genes. High genome collinearity within *Felidae* permitted alignment-based scaffolding onto the fishing cat (*Prionailurus viverrinus*) reference genome. Manul contigs spanned all 19 felid chromosomes with an inferred total gap length of less than 400 kilobases. Modified basecalling and variant phasing produced an alternate pseudohaplotype assembly and allele-specific DNA methylation calls; 61 differentially methylated regions were identified between haplotypes. Nearest features included classical imprinted genes, non-coding RNAs, and putative novel imprinted loci. The assembled mitogenome successfully resolved existing discordance between *Felinae* nuclear and mtDNA phylogenies. All assembly drafts were generated from 158 Gb of sequence using seven minION flow cells.

INTRODUCTION

Pallas's cat (*Otocolobus manul*), or the manul cat, is a small-bodied carnivore native to the montane grassland and shrubland steppe habitats of Central Asia (1). *O. manul's* wide geographic range spans varied climatic regions including the Caucuses Mountains, Mongolia and the Tibetan Plateau, but populations are concentrated at higher altitudes (2,3). Deemed the 'the grumpiest cat in the world' by the BBC documentary series *Frozen Planet II* (4), manuls are solitary hunters and subsist on a diet of small mammals (5). Prussian zoologist Peter Simon Pallas assigned the manul cat's taxonomic name as *Felis manul* in 1776 (6); the genus name *Otocolobus* was proposed in 1842 by Johann Fiedrich von Brandt (7) and formalized in 1907 based on skull morphology divergence from *Felis* (8).

Because of its wide home range and low population density, the conservation status of *O. manul* varies geographically. The International Union for Conservation of Nature (IUCN) Red List classifies the species as 'Least Concern' as of 2020 after being 'Near Threatened' in assessments from 2002 to 2016 (1, 9). However, *O. manul* is locally classified as endangered in several countries and either likely or confirmed extinct in some parts of its former range. Populations are also severely geographically fragmented, raising concerns for reduced effective population size and genome heterozygosity (10,11). The main threats to manul cats are anthropogenic, including poaching, habitat destruction, and the widespread use of rodenticides, which reduce prey populations and result in secondary poisoning of predators (12). A successful captive breeding program has led to *O. manul* being widespread in zoo collections around the world (13).

The manul cat is the sole extant species in the monotypic genus *Otocolobus*; phylogenetic analyses surrounding the relationship of this genus to other small-bodied

*To whom correspondence should be addressed. Tel: +1 612 624 7216; Email: cfaulk@umn.edu

© The Author(s) 2023. Published by Oxford University Press on behalf of NAR Genomics and Bioinformatics.
This is an Open Access article distributed under the terms of the Creative Commons Attribution-NonCommercial License (http://creativecommons.org/licenses/by-nc/4.0/), which permits non-commercial re-use, distribution, and reproduction in any medium, provided the original work is properly cited. For commercial re-use, please contact journals.permissions@oup.com

cats are ongoing. A phylogenetic study using select nuclear genes across the felid radiation placed *Otocolobus* as a sister lineage to the genus *Prionailurus*, a taxonomic group that includes the fishing cat (*P. viverrinus*) and leopard cat (*P. bengalensis*) among others (14). In contrast, a whole-mitogenome phylogeny placed *Otocolobus* closer to *Felis*, which includes the domestic house cat (*F. catus*) (15). Both studies are concordant with skull morphology data suggesting a Miocene divergence between *Pantheridae* and other cat lineages (16). Improved genomic resources for the manul cat will increase resolution for phylogenetic analyses within *Felidae*.

High-quality genome assemblies and comparative genomics experiments increasingly include data on the epigenome and repetitive DNA content (17–19). DNA methylation, the most well-studied epigenetic mark, is critical in embryonic development, genomic imprinting, and X-inactivation with additional influence on gene expression and transposable element (TE) suppression (20–25). Methyl-cytosines also exhibit a 2–3-fold increase in mutation rate relative to unmethylated cytosines via accelerated deamination (26), providing a molecular substrate for phenotypic change across evolutionary time. Long-read sequencing permits haplotype phasing based on DNA sequence variants, meaning that DNA methylation can also be segregated by parent of origin (27). This development is of paramount importance for genome-wide measurement of allele-specific DNA methylation, a signature of imprinted genes. Despite its biological significance, imprinting is chronically understudied due to technical limitations such as bisulfite fragmentation, multi-mapping, and reduced information complexity (28,29).

Widespread improvements in genome assembly quality reflect reduced sequencing costs, greater local computing power, and improved contiguity via long-read sequencing (30). Now within reach even for low-resource laboratories, these powerful tools can support conservation efforts for diverse animal species. Here, we provide a high-quality diploid nuclear genome assembly, updated mitogenome, and allele-specific methylation analysis for *O. manul,* all generated exclusively from Oxford Nanopore sequencing reads.

MATERIALS AND METHODS

DNA sample

A 5-year-old male manul cat residing at the Utica Zoo (Utica, NY, USA), Tater, was chosen for genome sequencing (Figure 1). Whole blood was collected by jugular venipuncture and shipped frozen, then thawed and combined with 2 volumes of DNA Shield (Zymo Research, Irvine, CA, USA). Genomic DNA was extracted using a Quick DNA Miniprep Plus kit (Zymo Research) yielding 25 μg of DNA from 200 ml of blood. DNA quality was checked using a nano-spectrophotometer (Implen N60, Munich, Germany) and run out on a 1% gel to visualize fragmentation and RNA contamination.

Library preparation. Seven gDNA library preparations were performed using the SQK-LSK110 kit (Oxford Nanopore Technologies, OX4 4DQ, UK) following a modified version of the manufacturer's instructions (Nanopore Protocol version GDE_9108_v110_revJ_10Nov2020). In the authors' modified version, each library prep used 3–5 μg of input DNA and was eluted with 45 μl of elution buffer (EB). Each elution was then split into three 15 μl aliquots to permit one initial flow cell loading step plus two reloads per library prep.

Figure 1. *Otocolobus manul* holotype photo depicting Tater, the 5-year-old male manul cat sampled for genome assembly.

Table 1. *O. manul* nanopore sequencing read summary. Reads were generated from 25 ug of DNA on seven minION flow cells over 21 total sequencing days

Number of reads	15349224
Number of bases	158 248 024 728
N50 read length (bp)	16 601
Longest read (bp)	379 006
Shortest read (bp)	38
Mean read length (bp)	10 309
Median read length (bp)	7099
Mean read quality (QV)	16.26
Median read quality (QV)	14.51

Sequencing. Sequencing was performed on seven R9.4.1 minION flow cells using Oxford Nanopore's minKNOW software (v22.05.5) and Guppy basecalling (v6.2.1). A total of three 15 μl DNA aliquots were loaded onto each flow cell with nuclease flushes between reloads per the SQK-LSK110 kit manual's 'Priming and loading' section. Each DNA aliquot was sequenced for 24 h for a total of 72 h of sequencing time per flow cell (21 total sequencing days). Guppy was set to fast basecalling during sequencing; post-hoc basecalling was performed using the 'super accuracy' model (r941_min_sup_g507). All assemblies were built using basecalls from the r941_min_sup_g507 model. Sequencing summary statistics (Table 1) and a histogram of read length data (Supplemental File 1) are provided.

Computational methods

Detailed pipeline information including software versions is provided in Supplemental File 2. The final assembly

required the use of cluster computing resources with 2TB of allocated random access memory (RAM); downstream analyses were performed on two local computers: one running Linux Ubuntu 20.04.1 with 128GB RAM, an NVIDIA 3090Ti graphics processing unit (GPU), and a 16-core, 32-thread AMD Ryzen 9 5950x central processing unit (CPU), and another running Linux Ubuntu (20.04.1) with 64GB RAM, two NVIDIA graphics cards (3080Ti and 2080Ti), and a 12-core, 24-thread Ryzen 9 3900x CPU. Abbreviated computational methods are included below.

Genome assembly and polishing. Because there is no single best assembly pipeline for mammalian genomes, we generated draft sequences using a variety of assemblers and polishers. Draft assemblies were generated locally or via institutional cluster computing using Flye (31), NextDenovo (github.com/Nextomics/NextDenovo), Shasta (32), and Raven (33). Polishing was performed with Medaka (github.com/nanoporetech/medaka) for consensus assemblies and Racon (34) or NextPolish (35) for non-consensus assemblies. Assembly quality was assessed by searching for *Carnivora*-specific genes with benchmarking universal single-copy orthologs (BUSCO) version 5.3.2 (36,37). The two highest-scoring assemblies from Flye and NextDenovo, respectively, were combined using the Quickmerge metassembler (38) to increase contiguity while preserving quality. The Purge Haplotigs pipeline was applied for reassignment and removal of allelic contigs (39,40). Software versions and calls to the assemblers are provided in Supplementary File 2.

Contamination detection. Unmapped raw reads were scanned for microbial DNA with Kraken2 (41) and Pavian (42). We manually inspected the final assembly for spurious contaminant contigs using GC content, unusually high (>1000×) or low (<1×) coverage depth, lack of BUSCO genes, and sequence similarity as metrics. Sequence similarity contamination screening was performed using Megablast versus NCBI's nucleotide (nt) database (43). Blobtools2 (44) was used to visualize GC content and read coverage (Supplemental Figure 1). An apparently chimeric 420 kb contig with >1000× coverage and no *Carnivora*-specific BUSCO genes matching *Felidae* by identity, ctg001250, was removed to generate the final primary assembly. Megablast hits to ctg001250 are provided in Supplemental File 3.

Coverage and quality statistics. Assembly coverage was assessed using Mosdepth version 0.3.345. K-mer quality value estimates were generated with Inspector, a tool built for long read data (45). We also applied Merqury, which was built for high accuracy short reads, to demonstrate its behavior on less accurate data (46).

Repeat identification. Repetitive DNA masking and classification was performed with RepeatMasker version 4.1.0 (47). Annotation using existing repeat classes, families and subfamilies was elected based on good representation of *Carnivora* in the Dfam version 3.5 open source repeat library.

Gene annotation. GeMoMa v1.8 and 1.9 (48,49) were applied to the primary assembly for homology-based protein prediction. First, version 1.8 was run with the *F. catus* gene annotation (GCF_018350175.1) used as the single reference; with the release of version 1.9, 'GeMoMaPipeline' was re-run with four felid gene annotations (*F. catus,* GCF_018350175.1; *P. viverrinus,* GCF_022837055.1; *P. uncia* GCF_023721935.1; *O. geoffroyi,* GCF_018350155.1) as a combined reference. Specific parameters are available in Supplemental File 2. 'GeMoMaPipeline' was also run on the *P. viverrinus* reference nucleotide assembly to assess the comparability of our *O. manul* output to NCBI's reference annotations. All predicted proteins were scored using BUSCO's protein mode and the carnivora_odb10 lineage dataset. Liftoff (50) was used with the *F. catus* (GCF_018350175.1) reference annotation to display gene features on differential DNA methylation plots for the *O. manul* assembly; DMR annotations were sanity checked by overlapping the GeMoMa and Liftoff annotation intervals. Proteins were not predicted for the Liftoff output.

Variant calling. Variant calling and phasing was performed using the PEPPER-Margin-DeepVariant pipeline (27). Variant statistics were generated using WhatsHap version 1.4 (51) and VCFtools version 0.1.17 (52). A consensus FASTA for the secondary haplotype was generated by applying all biallelic variants to the final assembly (considered the primary haplotype) with the consensus module of BCFtools version 1.15.1 (53). Runs of homozygosity and genomic demographics were assessed with SMC++ (54).

DNA methylation. DNA methylation (5 mC) at cytosine guanine dinucleotides (CpGs) was determined by re-basecalling QC-passed FAST5 files with a modified base configuration of GPU-mode Guppy (dna_r9.4.1_450bps_modbases_5mc_cg_sup). The final primary assembly was used as a reference. The resulting modified BAMs (modBAMs) were concatenated together into a single file, then sorted and indexed with Samtools (53). PEPPER-Margin-DeepVariant was then re-run to generate a haplotagged modBAM; this file and the primary assembly were used as input for ModBAM2BED version 0.6.2 (github.com/epi2me-labs/modbam2bed), which aggregates modified base counts to generate bedMethyl files. These files were then used as input for global and allele-specific methylation analysis.

Allele-specific DNA methylation was analyzed using the R package DSS developer version 2.43.2 (55–58). The package's two-group statistical comparison module 'DMLtest' was used to identify differentially methylated loci between the two haplotypes. The 'callDMR' module was then used with strict parameters ($P_{\text{threshold}} = 0.001$, delta = 0.5, minlen = 100, minCG = 15, dis.merge = 1500) to identify multi-CpG differentially methylated regions (DMRs).

DMR sequences were annotated via lifting of *F. catus* reference (GCF_018350175.1) gene features onto the *O. manul* assembly using Liftoff (50). The nearest feature to each DMR was then identified using AGAT (https://github.com/NBISweden/AGAT) and the closest module of BEDTools version 2.30.0 (59,60). DMRs annotated near genes with a 'LOC' symbol were additionally annotated with an alias

Table 2. Assembly statistics for selected *O. manul* drafts and reference genomes for fishing cat (*P. viverrinus*) and domestic house cat (*F. catus*). House cat is the felid species with the most high-quality genome assemblies; fishing cat is more closely related to *O. manul* by nuclear DNA phylogeny (14,15)

Assembly	Size (Gb)	Contigs/scaffolds/ chromosomes	Contig N50 (Mb)	BUSCO (% complete)	Depth	Technique
F. catus Fca126_mat1.0 (GCF_018350175.1)	2.42	110/71/19	90.7	95.5	76×	PacBio Sequel 2
P. viverrinus UM_Priviv_1.0 (GCF_022837055.1)	2.46	255/192/19	68.8	95.4	30×	PacBio Sequel
O. manul NextDenovo + Medaka	2.49	175/–/–	36.2	94.6	56×	Nanopore
O. manul Shasta + Medaka	2.47	714/–/–	26.3	94.1	56×	Nanopore
O. manul Flye + Medaka	2.49	1046/–/–	28.6	94.8	56×	Nanopore
O. manul Raven + Racon x2 + Medaka	2.50	568/–/–	9.2	94.7	56×	Nanopore
O. manul Quickmerge (Flye + NextDenovo) + NextDenovo	2.49	99/–/–	118.2	94.7	56×	Nanopore
O. manul Quickmerge + Purge Haplotigs	2.49	62/–/–	118.2	94.7	56×	Nanopore
OtoMan1.0	2.49	61/23/19	118.2	94.7	56×	Nanopore

or gene description, when available, via manual look up in NCBI's Gene database (https://www.ncbi.nlm.nih.gov/gene). Visualizations were generated using MethylArtist version 1.2.3 (61), which required haplotagging the PEPPER output with Longphase (62), and JBrowse 2 (63) to validate each DMR.

Mitochondrial genome. Nanopore reads were aligned to the *F. catus* mitogenome using Minimap2 (v2.22-r1101) (64,65). Aligned reads were then downsampled to 10 000 reads using Seqtk version 1.3-r106 (https://github.com/lh3/seqtk) and Flye (v2.9-b1768) in metagenome mode was used for assembly. Mitogenome annotation and manual rearrangement to start the circular mitogenome at COX1 was done previously (66). A mitogenome phylogeny was built using MUSCLE version 3.8 (67) for alignment and IQ-TREE version 1.6.12 (68) for bootstrapped maximum-likelihood tree inference.

Scaffolding. The contig-level assembly was scaffolded onto the fishing cat (*P. viverrinus*) reference genome with the scaffold module of RagTag (69). Alignment of the two genomes was assessed with Dot (github.com/marianattestad/dot) visualizations of Nucmer alignments (70). An ideogram of contig positions in the scaffolds was generated with the R pakcage chromoMap (CRAN.R-project.org/package = chromoMap).

RESULTS

Sequencing

We isolated DNA for the assembly from the whole blood of Tater, a captive-bred 5-year-old male manul cat residing at the Utica Zoo (Utica, NY, USA). A holotype photo is provided (Figure 1). DNA extraction yielded approximately 25 μg of total DNA. DNA was sequenced over 21 days using seven minION flow cells and base calling was performed using the GPU version of Guppy (v6.2.1). After default quality filtering, sequencing runs generated a total of 15.3 million reads and 158 Gb of sequence with a read N50 of 16.6 kb (Table 1). Of these reads, 66% had a quality score greater than Q20 (i.e. error rate of 1 in 100 base calls) and 20% were greater than Q30 (one error in 1000 base calls).

Initial assembly

We generated multiple *de novo* assemblies and chose the highest-quality result for further analysis based on BUSCO score (37) (Table 2). Twenty other *Felidae* reference genomes, including three domestic house cat (*F. catus*) assemblies, provided benchmarking (64,71–81). Other felid genomes ranged in sequencing coverage from 17× to 159× with an average BUSCO score of 89.56% and a median score of 95.1% (Figure 2); full felid genome assembly statistics used in this comparison are available in Supplemental File 3.

We ran multiple *de novo* assemblers with relatively low computational memory requirements (i.e. runnable with 64–128GB local RAM) including Flye, NextDenovo, Shasta, and Raven. Running Flye with the full sequencing read set on a mammal-sized genome required remote high-powered computing resources (≥400GB RAM), so Flye was also run locally with filtered read sets (Supplemental File 3). Filtering reads by length or quality reduced computational resources enough to run assembly software locally but resulted in slightly lower BUSCO scores, even after polishing with the full read set. Therefore, the full QC-passed read set was applied for both drafts used in the final assembly.

The two highest quality draft assemblies were generated by Flye and NextDenovo, both polished once with Medaka (https://github.com/nanoporetech/medaka). Of the two, the Flye sequence achieved the highest BUSCO completeness score for *Carnivora*-specific genes at 94.8% across 1000 contigs (Table 2). The NextDenovo assembly had fewer contigs (175) but a lower BUSCO score of 94.6%. Both sequences were appropriate in size for a felid genome at 2.49 Gb. A merged assembly was generated with Quickmerge to combine the best traits of both drafts (i.e. highest BUSCO score and largest contigs, respectively) (38). Merging parameters were set to reduce the likelihood of perpetuating errors or misjoining contigs, and the quality of each draft was assessed with Inspector (Supplemental File 2) (45). The Flye-Medaka draft's QV was 31.2 and the NextDenovo-Medaka draft's QV was 31.4. Visualizing alignments of the draft assemblies to each other and to the merge result additionally indicated that (i) the drafts were similar to one another pre-merge and (ii) the merge favored the Flye draft over the NextDenovo draft (Supplemental Figure 3). After merging,

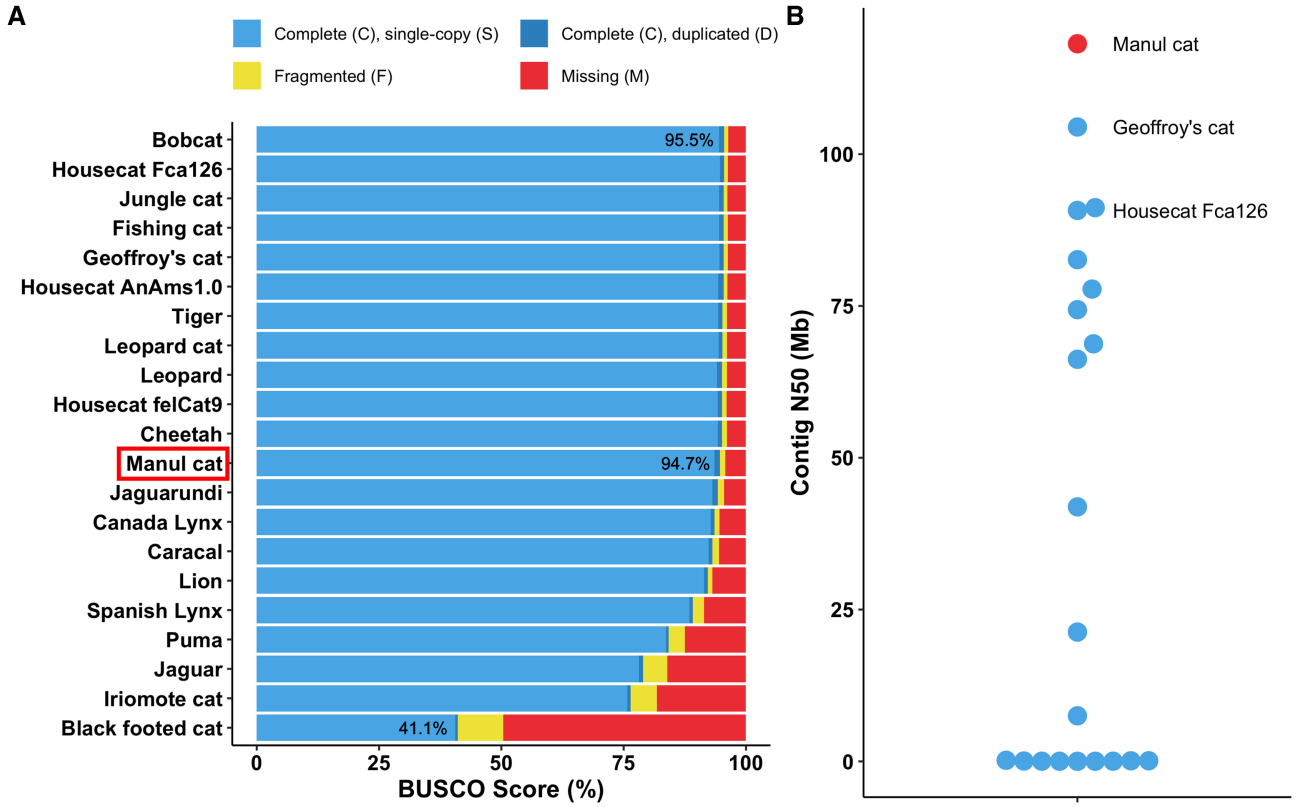

Figure 2. OtoMan1.0 is a near-complete and highly contiguous genome assembly for Pallas's cat (*Otocolobus manul*). (**A**) Felid reference assembly completeness was compared to our *O. manul* assembly by locally searching *Carnivora*-specific genes (carnivora_odb10) with BUSCO v5.3.2. OtoMan1.0, a nanopore-only assembly, ranked within 1% of the highest felid assembly BUSCO scores. (**B**) Contig N50 distribution for *O. manul* and felid reference assemblies. The *O. manul* assembly exhibits high contiguity (N50 = 118.2 Mb) when compared to other *Felidae* genomes, which differ minimally (~3 Mb) in size.

reassignment of allelic contigs was performed on the merge result with the Purge Haplotigs pipeline (39,40), bringing the number of contigs in the assembly down to 62.

Assembly curation and scaffolding

Recent nanopore-only genome assemblies have used anomalous coverage depth and expected GC content as a means of filtering alien contigs (82). Here, these parameters were assessed using Blobtools2 (44). There was one 420 kb contig with 1178× average coverage depth in the initial *O. manul* assembly, ctg001250. NCBI megablast matched the sequence to *Felidae*, making a contaminant or endoparasite source unlikely (Supplemental File 3). Examining sequencing read alignment to ctg001250 in JBrowse 2(63) revealed regions of typical (~60×) coverage interrupted by stretches covered by up to 4000 reads (Supplemental Figure 2). We concluded that ctg001250 was falsely contiguous based on a low number of reads spanning the high and low coverage areas, perhaps due to misplacement of interspersed repeats. Fifty percent of bases on ctg001250 were masked, and 40% were classified as LINE1 elements by RepeatMasker (Supplemental File 3). BUSCO score was intact following removal of ctg001250 (Table 2).

The final contig-level assembly, OtoMan1.0, was 2487293883 bp in length with 61 contigs, an N50 of 118.2 Mb, and a 94.7% BUSCO completeness score for *Carnivora* genes (Figure 2). Total genomic GC content was 41.87%. For comparison, 20 other *Felidae* reference genomes were locally reanalyzed with BUSCO v5.3.2 (carnivora_odb10). Our score of 94.7% places this nanopore-only assembly within 1% of the highest quality reference assemblies in *Felidae*. Additionally, the assembly's contig N50 was the highest among all assessed felid genomes. Half of OtoMan1.0 was covered by 8 contigs (L50) and the largest contig was 218.2 Mb (Supplemental Figure 4; Supplemental File 3). For reference, chromosome A1 in the current *F. catus* assembly is 239.4 Mb (RefSeq NC_058368.1). The shortest *O.* manul contig was 133 kb.

OtoMan1.0 was scaffolded onto the high-BUSCO fishing cat (*P. viverrinus*) reference genome (GCF_022837055.1) with the scaffold module of RagTag (69) (Figure 3). Fishing cat was chosen for alignment-based scaffolding due to (i) a lack of congenial species in *Otocolobus*, (ii) the genus sharing its most recent common ancestor with *Prionailurus* rather than *Felis* based on nuclear DNA (14,15) and (iii) the high BUSCO score of the *P. viverrinus* assembly. RagTag joined the 61 *O. manul* contigs into 23 scaffolds with 38 gaps, a total inferred gap length of 371685 bp, and a chromosome-level N50 of 151.9 Mb (Supplemental File 3). The scaffolds covered all 18 fishing cat autosomes, the X chromosome, and two unplaced BUSCO-containing fishing cat scaffolds (NW_025927612.1 and NW_025927619.1) (Supplemental Figure 3). Eight of the 18 cat autosomes

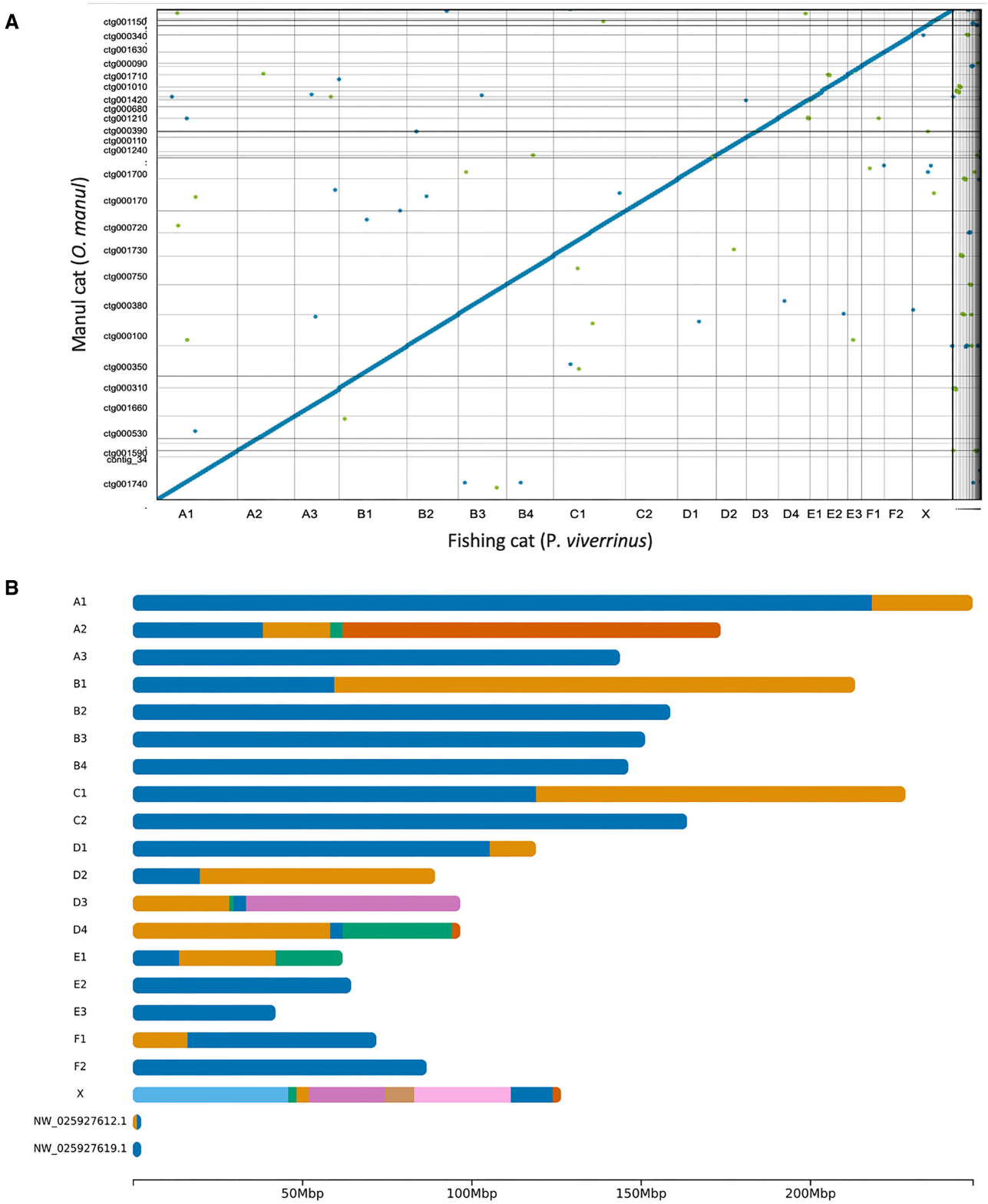

Figure 3. OtoMan1.0 cross-genus alignment and scaffolding. (**A**) Genome sequence alignment of the fishing cat (*P. viverrinus*) reference genome (GCF_022837055.1) and the contig-level nanopore assembly of *O. manul*, OtoMan1.0, was generated using Nucmer (70) and Dot (https://github.com/marianattestad/dot). The alignment quality reflects gross genome collinearity present across *Felidae* (80,83). (**B**) Ideogram of OtoMan1.0 scaffolds generated via alignment to the fishing cat (*P. viverrinus*) reference assembly (GCF_022837055.1). Color transitions represent breakpoints between contigs on the scaffold. All 19 felid chromosomes were covered by the OtoMan1.0 assembly, and eight autosomes (A3, B2, B3, B4, C2, E2, E3 and F2) were captured by single contigs. Manul contigs were also aligned to two BUSCO-containing fishing cat unplaced scaffolds while two of the 61 *O. manul* contigs were unplaced. Correlations between the fishing cat chromosome lengths and *O. manul* scaffold lengths are provided in Supplemental Figure 5.

Table 3. Repetitive DNA classification results for the manul cat (*Otocolobus manul*) genome assembly, OtoMan1.0, generated with RepeatMasker

	Element count	Total length (bp)	% of Genome covered
Total bases masked		863500886	34.72
Total interspersed elements		737829702	29.66
Retroelements	1596531	667340949	26.83
SINE:	470064	69243802	2.78
MIR	462472	68339639	2.75
LINE:	836683	488479415	19.64
LINE1	468806	391204655	15.73
LINE2	312177	84936852	3.41
L3/CR1	41423	8915823	0.36
RTE	13010	3218808	0.13
LTR:	289784	109787884	4.41
ERVL	88371	39831330	1.60
ERVL-MaLRs	148224	51463432	2.07
ERV_classI	28861	12430326	0.50
DNA elements:	356331	69720741	2.80
hAT-Charlie	198573	36753878	1.48
TcMar-Tigger	55938	14630791	0.59
Unclassified	3794	597860	0.02
Small RNA	146099	11047204	0.44
Simple repeats	1677548	79649218	3.20
Low complexity	647428	34786006	1.40

(44%) were captured by single contigs in our assembly (Figure 3B), but two *O. manul* contigs were left unplaced. One of the two unplaced contigs was 593 kb in length and had 98.5% identity to a fragment of the 1.9 Mb *F. catus* Y chromosome (51% query coverage) when assessed with NCBI Megablast (43); the animal sampled to build UM_Priviv_1.0 was female. The second unplaced *O. manul* contig was 187 kb in length and exhibited high but discontiguous BLAST identity to *F. catus, P. bengalensis* and other felid sequences.

Repetitive DNA

Repetitive DNA, particularly interspersed repeats, are valuable drivers of genetic diversity in vertebrates (84,85). Since carnivores are well-represented in transposable element (TE) databases, we classified and annotated *O. manul* repetitive DNA with RepeatMasker (Table 3) (47). Overall, 34.72% of the assembly was classified as repetitive DNA, with a majority of retroelements (26.83%) and fewer DNA elements (2.8%), simple repeats (3.2%), and low-complexity regions (1.4%). These results are consistent with the dominance of retroelements in mammalian genomes (86,87). Local analysis of other cat assemblies with RepeatMasker indicated that OtoMan1.0's repeat complement was consistent with other members of *Felidae* (Figure 4). Conservation of global repeat content in this clade was high: the 18 analyzed species varied by 3.67% for total bases masked, 2.72% for LINE content, 0.16% for SINE content, and 0.15% for DNA element content (Supplemental File 3).

Diploid genome

After read phasing OtoMan1.0 with the PEPPER-Margin-DeepVariant pipeline (27), approximately 83% of the assembly was covered by 6613 phase blocks with a block NG50 of 0.53 Mb (Supplemental File 3). As expected, most variants were single nucleotide variants (SNVs) and small insertions and deletions, with fewer large indels. Of 2045611 heterozygous variants detected, 1 561 420 (76.3%) were phased and 1 087 364 (53.2%) were phased, biallelic SNVs. The transition-transversion ratio (Ts/Tv) for biallelic SNVs was 2.12, in line with highly methylated mammalian genomes (Supplemental File 4). The software employed for variant calling does not detect inversions. The scaffolded primary assembly was deposited as BioProject PRJNA885133 and the contig-level alternate haplotype assembly as BioProject PRJNA889808.

An alternate pseudohaplotype assembly was generated by switching biallelic variants from the PEPPER variant call file into the primary, contig level assembly using the 'consensus' module of BCFtools (53). The resulting sequence was 2 484 282 002 bp in length with a contig N50 of 118.0 Mb and 94.8% BUSCO score.

We estimated diploid assembly quality using Inspector, a reference-free, k-mer-based tool built for long reads (45)**.** Inspector's estimated QV for the primary contig-level assembly was 31.3 (99.93% accuracy) with a *k*-mer completeness score of 97.9% (Supplemental File 3). Inspector additionally scored the pre-merge assembly drafts from Flye and NextDenovo at Q31.2 and Q31.4, respectively. Inspector also includes a correction module for structural and base-level errors, but running it reduced OtoMan1.0's BUSCO from 94.7% to 93.6% and inflated the reported number of structural errors.

We additionally ran Merqury on the diploid assembly (46). Merqury was built for high accuracy short reads, and lower accuracy read sets are more likely to produce QV overestimates. Still, this use case of a popular quality estimation tool is unreported in the literature. On default settings, Merqury gave OtoMan1.0 a *k*-mer completeness score of 97.5% and quality score of Q45.3 (Supplemental File 2). We also ran Merqury's 'best_k' script, which is intended to provide an ideal k-mer length for analysis based on genome size and read error rate. Given our median read error rate of 0.035, 'best_k' suggested k = 19; this value further inflated the QV to 53.2 from the original Q45.3 using the default $k = 21$. Despite these potential QV overestimates, Merqury's histogram output indicated that most small k-mers were excluded from the final assembly, appearing only in the read set (Supplemental Figure 6).

Lastly, genome heterozygosity and effective population size for *O. manul* were assessed using variant calls. Heterozygosity was 0.048% based on the number of called heterozygous SNVs (1 184 174) divided by the total callable bases in the contig-level primary assembly and 0.082% using all 2045611 heterozygous variants combined (SNVs and indels). Population history inferences for *O. manul* based on genomic runs of homozygosity were conducted with SMC++ (54). The results suggested an effective population size (N_e) near 10 000 with recovery from a bottleneck approximately 3000 generations ago (Supplemental Figure 7).

Annotation

Homology-based gene annotation was performed on OtoMan1.0 with Gene Model Mapper (GeMoMa) versions 1.8 and 1.9. The *F. catus* RefSeq annotation

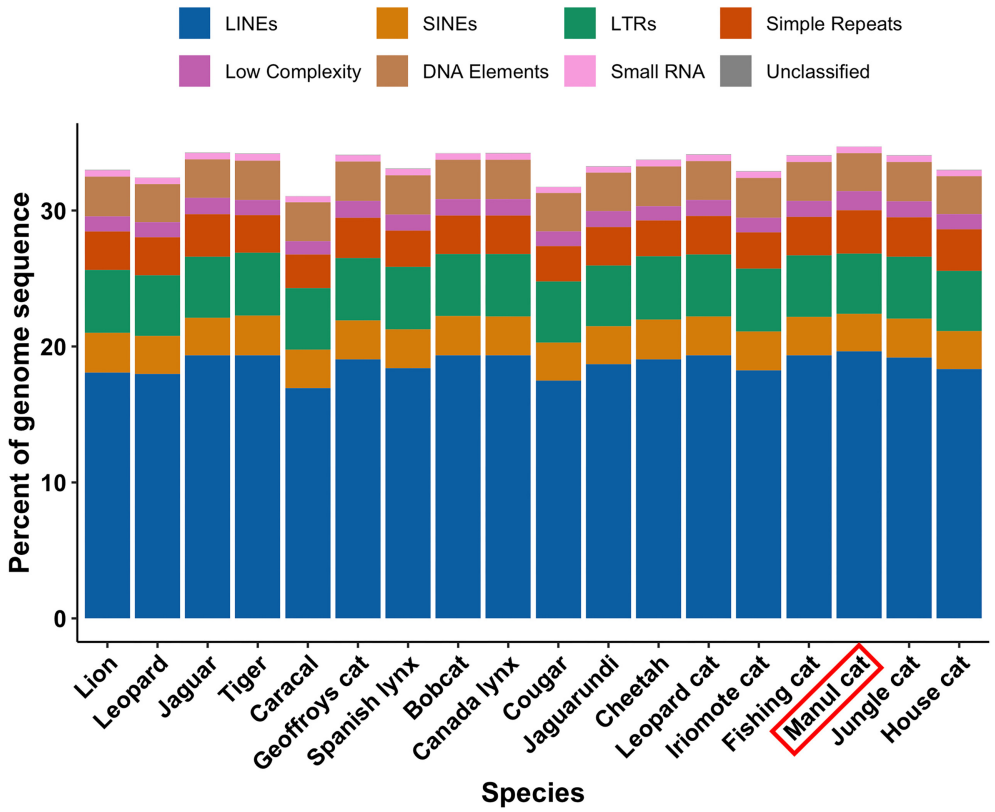

Figure 4. Repetitive element content of the assembled *O. manul* genome and 17 other felid species assessed with RepeatMasker (47). Manul cat repeat content was highly similar to other members of *Felidae* and dominated by retroelements.

(GCF_018350175.1) served as the reference for our initial v1.8 run, generating 21909 amino acid predictions with an 86.2% protein BUSCO score (Supplemental File 2). A second prediction was generated using the *P. viverrinus* reference annotation as reference (GCF_022837055.1) instead, but BUSCO completeness was lower at 85.3%.

With the release of GeMoMa version 1.9, we re-ran GeMoMaPipeline on OtoMan1.0 using four felid reference annotations (*F. catus,* GCF_018350175.1; *P. viverrinus,* GCF_022837055.1; *P. uncia* GCF_023721935.1; *O. geoffroyi,* GCF_018350155.1) for a single prediction. The resulting protein BUSCO score was only slightly higher at 88.2% (Supplemental File 2).

To benchmark the GeMoMa software, we also predicted proteins for the *P. viverrinus* reference nucleotide assembly using *F. catus* as the annotation reference in GeMoMa v1.8. The resulting protein BUSCO score was 86.8%, within 1% of OtoMan1.0's original protein score (Supplemental File 2). Both scores fall below our locally calculated BUSCO values for the *F. catus* (99.6%) and *P. viverrinus* (99.2%) protein annotations, which were generated with NCBI's Eukaryotic Gene Annotation Pipeline.

DNA methylation

Nanopore instruments can detect native DNA modifications via modified pore signals compared to the unmodified base. Here, 5-methylcytosine (5mCG) base modifications were called using Guppy with the contig-level assembly as an alignment reference, generating methylation data for 33085506 cytosine-guanine dinucleotides. Similar to other mammals (88), global DNA methylation at CpG dinucleotides was high in *O. manul* at 78.2%.

Allele-specific methylation, a mechanism that facilitates monoallelic gene expression in genomic imprinting, was assessed by calling differentially methylated regions (DMRs) between *O. manul* pseudohaplotypes with DSS (55). Strict calling parameters (i.e. methylation delta at least 50%, 100 bp length, at least 15 CpGs) yielded 91 unique loci (Table 4). Visualization of haplotagged read alignments at each DMR facilitated the discovery of 30 false positive loci, where apparent read misalignment for one of the two haplotypes led to a called DMR via a lack of CpGs on one allele. Of the original 91 loci, 61 (67%) were deemed true DMRs following manual inspection (Supplemental File 3). The validated DMRs had a mean length of 969 bp and a mean of 118 CpGs.

Validated DMRs were annotated by lifting *F. catus* reference gene features onto the contig-level *O. manul* assembly and querying the nearest gene with BEDTools (60). This method captured a number of classical imprinted loci described in humans and other animals, including GNAS, NNAT, IGF2, IGF2R, KCNQ1, MEST and ZDBF2 (Table 4) (89–93). In total, 41 validated DMRs directly overlapped 49 genes while non-overlapping DMRs fell between 165 bp and 56.7 kb away from the nearest feature. Putative novel imprinted loci, or DMRs near a feature not previously described as imprinted, including a 595 bp, 106-CpG

Table 4. Summary statistics and nearest gene feature data for differentially methylated regions (DMRs) called between *O. manul* pseudohaplotyes. Gene annotation data were lifted onto the OtoMan1.0 assembly from *F. catus* (F.catus_Fca126_mat1.0) and the nearest feature to each DMR was found with BEDTools (60). DMRs were validated visually using read pileup data. Statistics are shown for validated DMRs. Gene aliases are included in parenthesis

Initial DMRs	91
Validated DMRs	61
Mean length (bp)	969
Median length (bp)	705
Mean number of CpGs	118
Median number of CpGs	75
Mean absolute difference in methylation (%)	71.15
Median absolute difference in methylation (%)	69.67
Mean distance to gene feature (bp)	3463
Median distance to gene feature (bp)	0
Nearest genes to DMRs (symbol)	MXRA7, KCNQ1, IGF2, LOC109492247, CTSD, CAMK1G, IGF2R, LOC123383330, LOC109499294, LOC111560210, HERC3, NAP1L5, LOC109500454, BNC1, IGF1R, LOC109500537, UBE2Q2, LOC102900156, KLC1, SOCS6, LOC123378902, MEST, LOC109497613, VWDE, HSPG2, ST8SIA6, LOC111561284, SNU13, ATP4A, LOC123382347, INPP5F, LOC101093666, LOC102899880, LOC101083149, ATP6V1H, FAM110B, LOC109495939, BLCAP, NNAT, LOC102900772 (NESP55), LOC101098453 (GNAS), LOC109497888, CALCB, LOC123380523, GNA12, LOC105261300, TEKT5, ZDBF2, CMKLR2 (GPR1)

DMR in the first exon of Von Willebrand factor D and EGF domain-containing protein (VWDE). Representative DMRs are shown in Figure 5. The mean absolute difference in methylation between the two pseudohaplotypes at DMRs was 71.15%. Most validated DMRs (44 of 61, 72.1%) were hypomethylated on the alternate pseudohaplotype, while 17 were hypermethylated.

Of the 61 validated DMRs, 12 (19.67%) occurred in one contiguous 33.2 kb region on feline chromosome C1 (Figure 5). All DMRs in the region were hypomethylated on pseudohaplotype 2. The region fell directly upstream of two genes, chemerin chemokine-like receptor 2 (CMKLR2) on the positive strand and zinc finger DBF-type containing 2 (ZDBF2) on the negative strand. ZDBF2 is a canonical imprinted gene expressed paternally in most human and mouse tissues (94); imprinted expression of CMKLR2, a paralog of opioid receptor kappa 1 (OPRK1), has not been reported, but expression of its antisense transcript (GPR1AS) is imprinted in human and mouse placenta (95).

Mitochondrial genome

The mitochondrial genome assembly built using Flye in metagenome mode contained one circular contig 17 097 bp in length with 800× read coverage (Figure 6). Megablast revealed a 99.7% nucleotide identity match to a previously assembled *O. manul* mitogenome (Supplemental File 3) (98). However, our assembly was longer than this previous manul mitogenome assembled from Sanger sequencing reads in 2019, which was 16 672 bp (GenBank MH978908.1). The 400 bp gap identified between our assembly and the 2019 version was located in the non-coding D-loop region of the mitogenome, making misassembly less likely than in the case of a large genic insertion. A 2015 Illumina mitogenome assembly for *O. manul* was closer to our assembly's length at 17 009 bp (KR132585.1), but identity and query coverage were lower. From our mitogenome, a new phylogeny was built using tiger (*Panthera tigris*) as the outgroup. The resulting phylogeny matched previous nuclear DNA trees, with *Otocolobus* sharing its most recent ancestor with *Prionailurus* (14) in contradiction of a 2016 mitochondrial phylogeny that placed *Otocolobus* closer to *Felis* (15). The mitogenome was deposited as part of the scaffolded primary assembly at BioProject PRJNA885133.

DISCUSSION

Here, we have produced a highly contiguous diploid nuclear genome assembly, mitogenome, and allele-specific DNA methylation dataset for the manul cat (*Otocolobus manul*) via standalone nanopore sequencing. With 61 contigs and a contig N50 of 118.2 Mb, the assembly was more contiguous than any other *Felidae* reference genome to date before scaffolding. The felid clade is particularly well-suited for cross-genus scaffolding due to conserved genome collinearity among its members; our scaffolding strategy may not yield such unambiguous results in other animal families (80,83). Comparing our primary assembly to the original read set with Inspector yielded a *k*-mer completeness score of 97.9% and QV of 31.3 (99.93% accuracy). Using a single sequencing technology without parental data, this QV score approaches the 'platinum-quality' reference genome standard of Q40 (99.99% accuracy) established by the Vertebrate Genomes Project (VGP) (77,99,100). Our assembly exceeds VGPs other benchmarks of contig N50 $\geq$ 1 Mb and chromosomal scaffold N50 $\geq$10 Mb by 118-fold and 15-fold, respectively. Merqury yielded a higher QV estimate of 45.3 on default settings, but the score is likely an overestimate due to a relatively high read error rate. Still, Merqury's k-mer spectra histograms indicated that most small k-mers were excluded from the final assembly, suggesting that our coverage depth was able to overcome the read set error rate to produce a high-quality genome.

Our assembly's BUSCO score for *Carnivora*-specific genes, 94.7%, also fell within 1% of the most complete felid genomes. Importantly, BUSCO values were re-calculated locally using an updated version of the program (v5.3.2), leading to lower scores overall compared to those currently displayed on NCBI's Genome pages (v4.1.4). The described genome, OtoMan1.0, reflects the continued, rapid

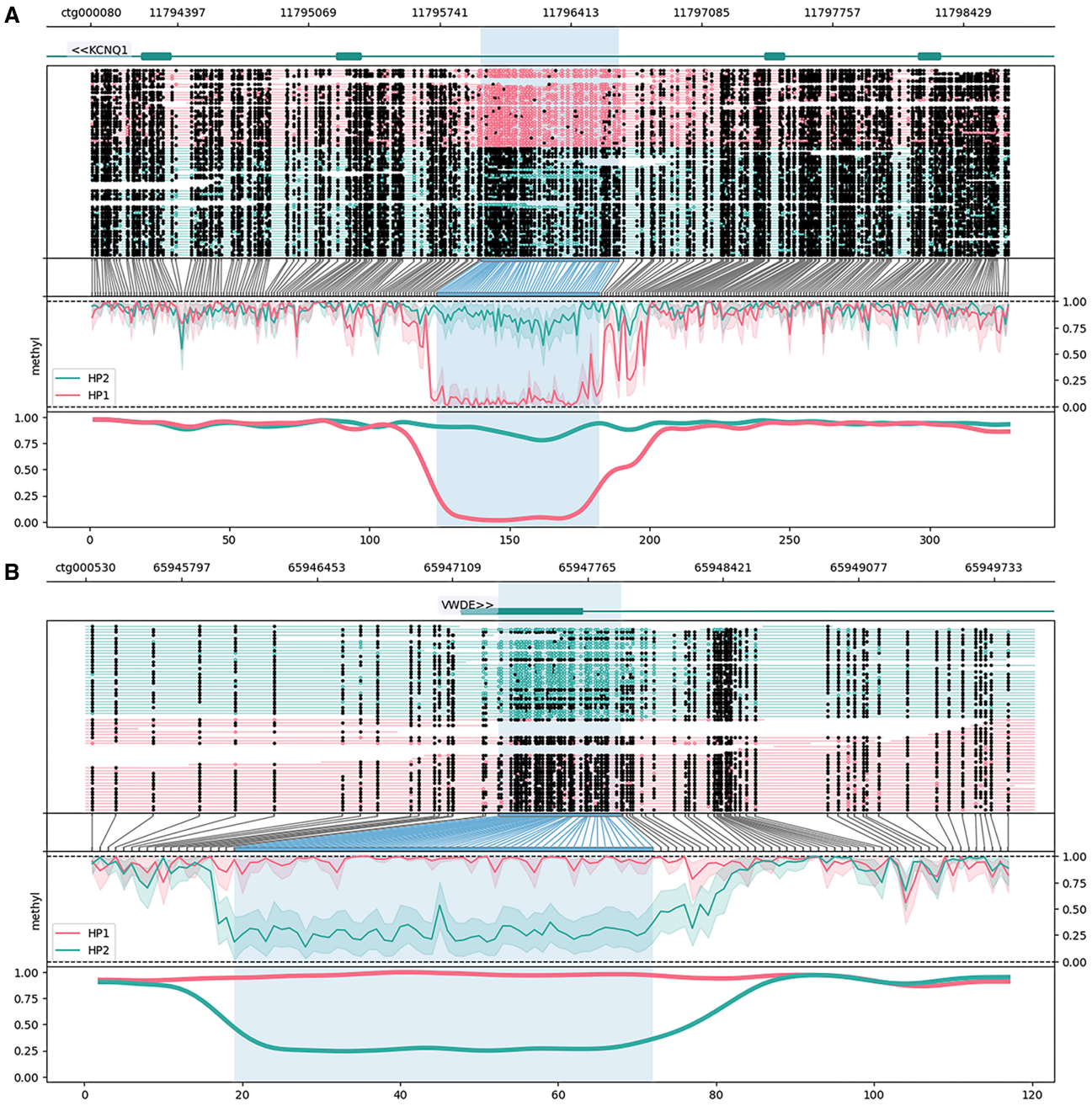
A
ctg000080
11794397
11795069
11795741
11796413
11797085
11797757
11798429
<<KCNQ1
methyl
HP2
HP1
1.00
0.75
0.50
0.25
0.00
0
50
100
150
200
250
300
B
ctg000530
65945797
65946453
65947109
65947765
65948421
65949077
65949733
VWDE>>
methyl
HP1
HP2
1.00
0.75
0.50
0.25
0.00
0
20
40
60
80
100
120

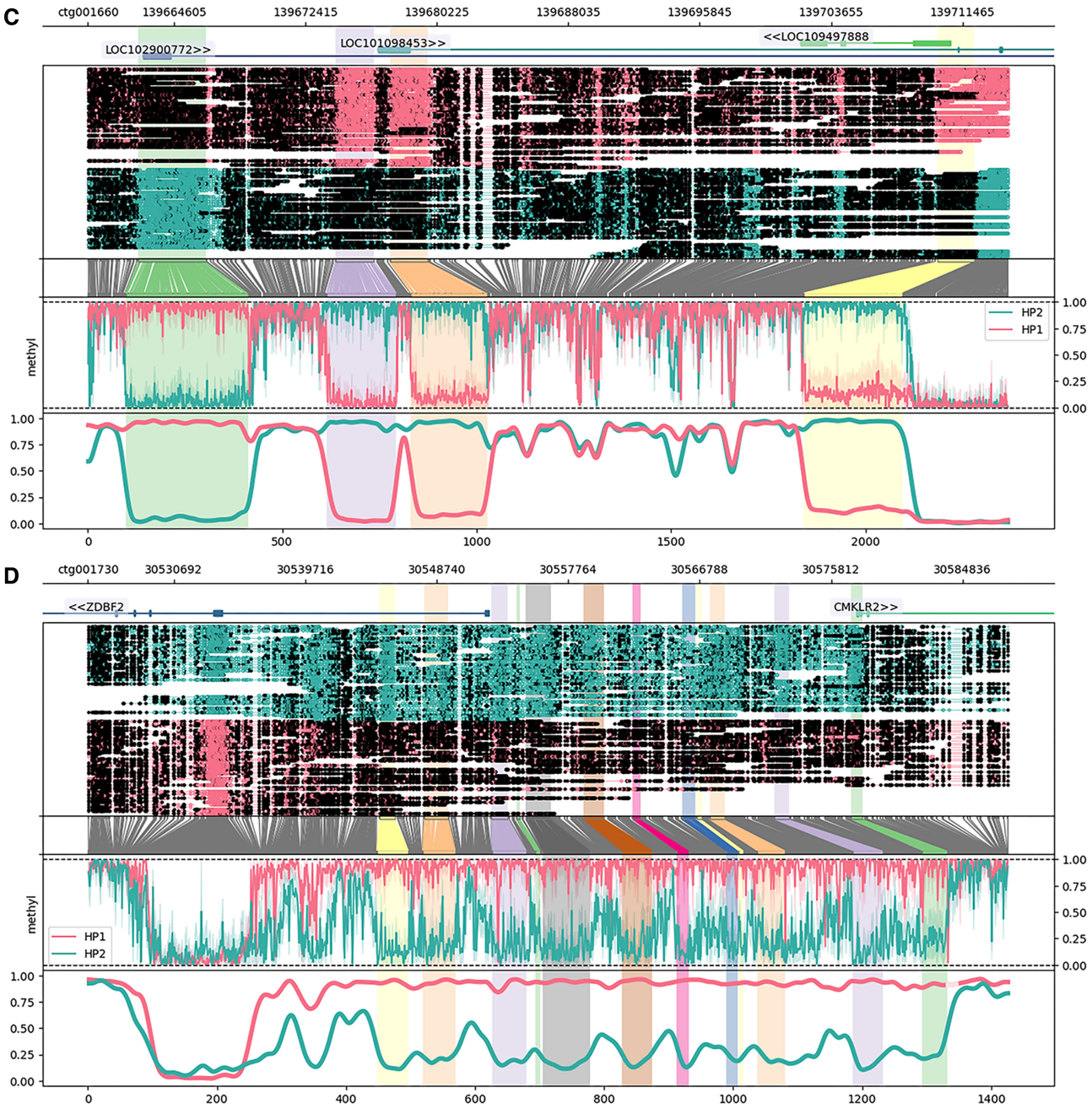

Figure 5. Allele-specific DNA methylation at differentially located loci (DMRs) called between *O. manul* assembly pseudohaplotypes assembled from a whole blood sample. DMRs were visualized with the package Methylartist (61). Annotation of the 61 manually validated DMRs was accomplished by lifting gene coordinates from the *Felis catus* reference assembly (F.catus_Fca126_mat1.0) onto OtoMan1.0 and finding the nearest feature. The results revealed (**A**, **B**) singleton DMRs and (**C**, **D**) multi-DMR clusters within and near genes. Genes overlapping DMRs included previously described imprinted loci such as (A) potassium voltage-gated channel subfamily Q member 1 (KCNQ1) and (B) the guanine nucleotide-binding protein G(S) subunit alpha (GNAS) complex locus (aliases LOC101098453, LOC102900772). DMRs also overlapped genes not previously reported as imprinted, including (C) von Willebrand factor D and EGF domains (VWDE), a protein with predicted involvement in anatomical development (96). (D) The most notable locus was a 33.2 kb region containing 12 DMRs all hypomethylated on pseudohaplotype 2. The DMRS overlapped the 5' end of a classical imprinted gene, zinc finger DBF-type containing 2 (ZDBF2), on the negative strand and the 5' end of chemerin chemokine-like receptor 2 (CMKLR2) on the positive strand. The CMKLR2 antisense RNA (CMKLR2AS; alias GPR1AS), which is not annotated in *F. catus*, exhibits imprinted expression in the human placenta (97).

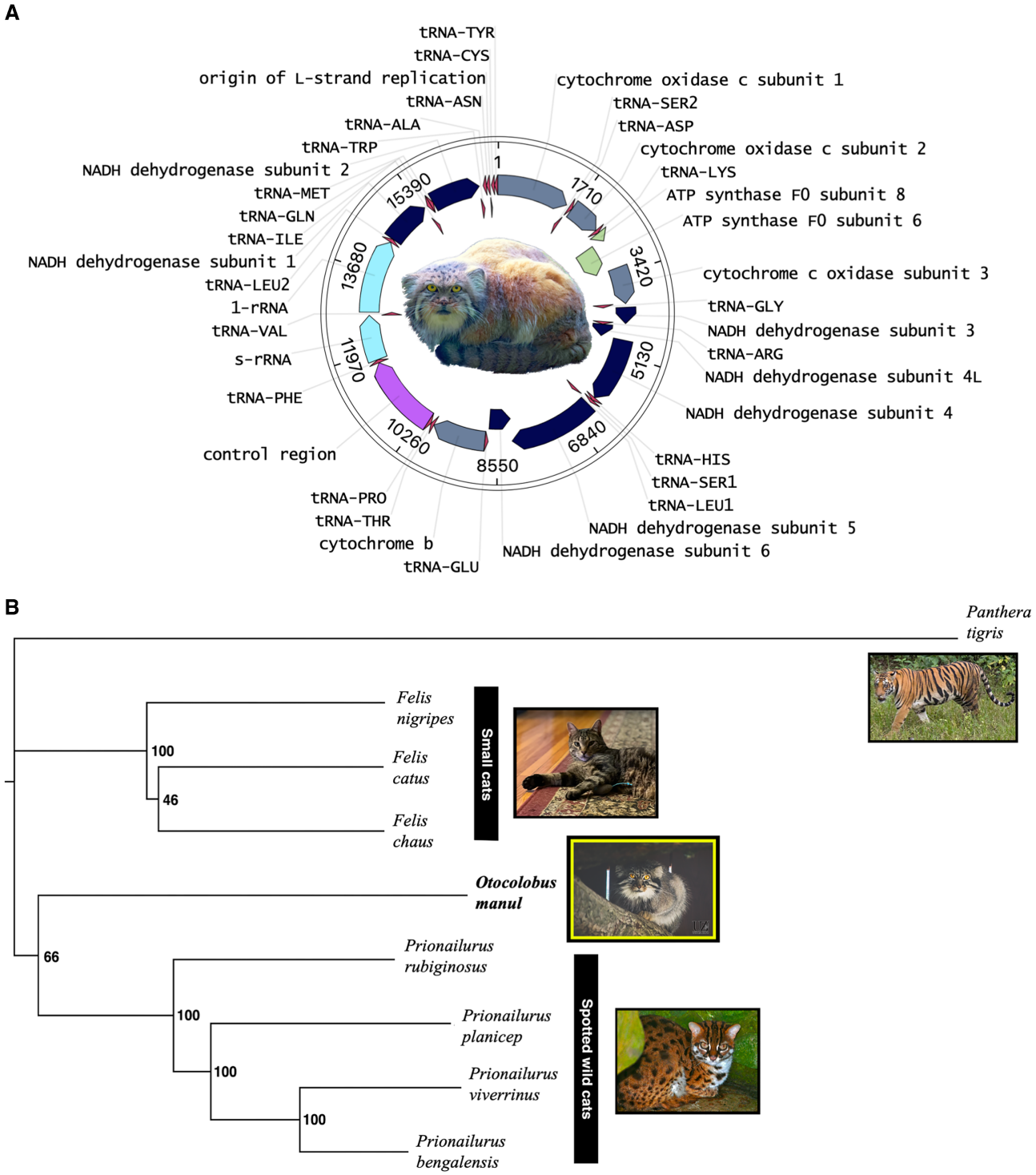

Figure 6. Nanopore mitochondrial genome assembly of *O. manul* and felid mtDNA phylogeny. (**A**) The circular length of the built *O. manul* mitogenome assembly was 17 097 bp; read coverage was 800×. (**B**) Phylogenetic relationships of *O. manul* were derived through bootstrapped maximum likelihood comparison of the assembled mitogenome to existing Felidae references. In contrast to previously published mtDNA for *O. manul* (98), the current tree matches those generated through analysis of nuclear DNA (14).

improvement of assembly pipelines and the necessity of long-read sequencing for generating contiguous, high-quality reference genomes (101–104). Our results also provide evidence against concerns for low nanopore-only assembly quality due to sequencing error rates.

Repetitive elements have been minimally explored in felids despite their high genome occupancy and role in phenotype evolution (105–108). SINE element insertions are major sources of genomic diversity in canids, with links to multiple phenotypes in domestic dogs (*Canis lupus familiaris*) including early retinal degeneration, polyneuropathy, myopathy, and merle coat color (109–115). While global repeat content is strongly conserved across *Felidae* based on our analysis, individual repeat family activity is potentially variable and relevant to intra- and inter-species conservation. In a biomedically relevant example, domestic cats but not large cats possess an infectious endogenous retrovirus (ERV), RD-114, which can contaminate vaccines manufactured with feline cell lines and infect experimentally inoculated dogs (116–118). Long-read sequencing enables more accurate investigation of genomic repeat content; single reads can span full TEs and capture unique flanking host sequences, reducing multi-mapping issues inherent in short read assembly (119–121).

Nanopore sequencing permits native DNA methylation detection alongside DNA base calls, combining genome assembly and epigenome analysis into one step at the bench top. The epigenome is responsive to an animal's environment and shifts in a predictable manner across the life span (122,123). Here, we present a phased methylome and allele-specific DNA methylation analysis for *O. manul*. Our differentially methylated region (DMR) detection criteria were relatively strict in an effort to reduce false positives and yielded 61 validated loci. We successfully captured a number of classical imprinted genes including NESP55/GNAS, KCNQ1, NNAT, IGF1R and IGF2/H19 (124–128). IGF2R contained a DMR in this study suggestive of imprinted expression; this gene is maternally expressed in dogs (129,130) while monoallelic expression appears to have been lost in the primate lineage (131). Putative novel imprinting loci were also identified in genes such as Von Willebrand factor D and EGF domain-containing protein (VWDE), a paralog of fibulin 2 (FBLN2) required for multi-tissue limb regeneration in the axolotl (*Ambystoma mexicanum*) (132). A 2012 study found that 40% of human genomes deposited by the 1000 Genomes project (www.1000genomes.org) carried at least one loss-of-function mutation in VWDE (133). This locus and others were evaluated as distinct from 30 false DMRs, where misassembly resulted in a lack of CpGs on one pseudohaplotype. This phenomenon is not detectable to the DMR calling software *DSS*, necessitating manual curation; humans have over 200 imprinted genes (127,134) meaning our DMR calling parameters likely also introduced false negatives. Although imprinted gene expression cannot be predicted based on methylation data alone, this assembly provides a high-quality alignment reference for future transcriptomic analyses in *O. manul*. Future comparative investigations in diverse species will enrich our functional understanding of the allele-specific methylation mechanism.

Detection of low genome heterozygosity in this captive-bred *O. manul* individual is a concerning but valuable insight for both zoo breeding programs and wild population management. At 0.048%, our estimate of heterozygosity using biallelic pseudohaplotype SNVs was similar to the critically endangered Amur tiger (*Panthera tigris altaica*), a species that experienced a severe population bottleneck in the 1940s with a current estimated population of 400 animals (135–138). In contrast, the manul cat population is estimated at 58 000 individuals (1). Although captive breeding programs are a crucial tool in global conservation, a small pool of founder animals inevitably leads to reduced genetic diversity. Practices like sperm biobanking have the potential to support captive population genetic quality, but such systems are underutilized (139). Fortunately, our estimate of effective population size using runs of homozygosity was relatively large at $N_e = 10\,000$. Results also suggested that manul cats experienced a crash in genetic diversity, but that this event was in the relatively distant past (~10000 years ago); effective population size appears to have continued recovering despite anthropogenic challenges to the species. Given the large, low-density geographic range and solitary social strategy of *O. manul*, it is unclear whether these values are typical across the entire population.

While largely conserved among metazoans, mitogenomes also contain structural and nucleotide variation that can serve as phylogenetic markers (140). Their smaller size, relative to nuclear genomes, make them an attractive tool in phylogenetics. However, incongruities between mitogenome and nuclear DNA phylogenies can occur due to uniparental inheritance of organelles (141), horizontal gene transfer (142), or incomplete lineage sorting (143). Previously, an *O. manul* mitogenome assembly placed *Otocolobus* as a sister taxa to the *Felis* clade (15). The mitogenome assembly presented here contains a previously unidentified 400 bp gap in the D-loop control region; a new phylogenetic analysis placed *O. manul* closest to *Prionailurus* in agreement with the nuclear genome phylogeny (14). This finding suggests that *O. manul* nuclear DNA and mtDNA have similar phylogenetic histories. Recently, felid mitogenomes were used to investigate the contribution of a wild cat to domestication of *F. catus* (144). Using our mitogenome assembly, a similar study could investigate introgression among wild Asian cats (i.e. *O. manul* and *Prionailurus spp.*) and between wild and domestic cats in this region. Hybridization among cat species could have important implications for genetic diversity and conservation. Notably, evidence of hybridization among domestic and wild cats is found in South Africa and Europe, and is related to human population density in proximate spaces to wild cat habitat (145,146).

Long-read sequencing in general has been critical for increased genome assembly quality, but the portability and cost-effectiveness of nanopore sequencing make it particularly valuable for reducing barriers to entry in genomics (82,104). Still, assembly of mammalian-sized genomes (3+ Gb) can exceed computational and financial resources available to small laboratories. Even Flye, an efficient assembler (31), required distributed computing resources when using our full read set (Table 2; Supplemental File 3). Unequal access to such resources can inadvertently perpetuate 'parachute science' and limit the participation of

researchers from historically colonized countries in endemic species conservation (147–149). However, we were able to build *O. manul* assemblies locally using a subset of the longest reads with only a small reduction in BUSCO score (Supplemental File 3). On-demand cloud computing resources such as Amazon Web Services (AWS) are also increasingly affordable, eliminating the necessity of access to a university cluster. We hope that the provided data and computational pipeline will be useful resources for *O. manul* conservation as well as for other small groups assembling mammal genomes.

DATA AVAILABILITY

DNA sequencing reads are available in FASTQ format in the Sequencing Read Archive repository (https://www.ncbi.nlm.nih.gov/sra) under submission SRR22085263. The scaffolded primary assembly (including mitogenome) is available as BioProject PRJNA885133; the contig-level alternate assembly is available as BioProject PRJNA889808. Modified base calls (DNA methylation) are also available under BioProject PRJNA885133. Sample data are available as BioSample SAMN31076064. Gene annotation, variant calling, and DNA methylation data are available by request.

SUPPLEMENTARY DATA

Supplementary Data are available at NARGAB Online.

ACKNOWLEDGEMENTS

We thank the Utica Zoo and Tater for providing the whole blood sample used in this study. For Figure 6B, leopard cat photo credit goes to Bernard Dupont and tiger photo credit to Charles J. Sharp, both under Creative Commons licenses.

FUNDING

United States Department of Agriculture National Institute of Food and Agriculture [HATCH AES MIN-16–12 to C.F.]; Norn Group [Longevity Impetus Grant to C.F.]; National Institutes of Health [R21 AG071908 to C.F., L70 AG079467-01 to N.F., T32 OD010993 to N.F.]; National Science Foundation [IOS 1556396 and IOS 1754437 to M.K.D.]
Conflict of interest statement. None declared.

REFERENCES

1. Ross,S., Barashkova,A., Dhendup,T., Munkhtsog,B., Smelansky,I., Barclay,D. and moqanaki,E. (2019). *Otocolobus Manul*. http://www.10.2305/iucn.uk.2020-2.rlts.t15640a180145377.en, (10 February 2023, date last accessed).
2. Gittleman,J.L. (1993) Heptner, V.G. and Sludskii, A.A. 1992. Mammals of the soviet union. volume II, part 2. Carnivora (hyaenas and cats). Smithsonian Institution Libraries and National Science Foundation. *J. Mammal.*, **74**, 510–511.
3. Murdoch,J., Tserendorj,M. and Reading,R. (2006) Pallas' cat ecology and conservation in the semi-desert steppes of mongolia. *CAT News.*, **45**, 18–19.
4. BBC. (2022) The grumpiest cat in the world. https://www.bbc.co.uk/programmes/p0cz5p0y, (10 February 2023, date last accessed).
5. Ross,S., Munkhtsog,B. and Harris,S. (2010) Dietary composition, plasticity, and prey selection of Pallas's cats. *J. Mammal.*, **91**, 811–817.
6. Pallas,P.S. (1776) In: *Reise durch verschiedene provinzen des russischen reichs. Vol. Reise aus sibirien zurück an die wolga im 1773ten jahr*. Kayserliche Academie der Wissenschafen, St. Petersburg, Russian Empire.
7. Brandt,J. (1842) Observations sur le manoul (*felis manul pallas*). *Bull. Sc. Ac. Imp. Sc. St. Petersb.*, **9**, 37–39.
8. Thomas,O. and Wroughton,R.C. (1907) 3. The rudd exploration of South Africa.—VII. List of Mammals obtained by Mr. Grant at Coguno, Inhambane. *Proc. Zoo Soc. Lond.*, **77**, 285–306.
9. Ross,S., Barashkova,A., Farhadinia,M., Appel,A., Riordan,P., Sanderson,J. and munkhtsog,B. (2014) *Otocolobus Manul*. http://www10.2305/iucn.uk.2016-1.rlts.t15640a87840229.en, (1 February 2023, date last accessed).
10. Spong,G., Johansson,M. and Björklund,M. (2000) High genetic variation in leopards indicates large and long-term stable effective population size. *Mol. Ecol.*, **9**, 1773–1782.
11. Palstra,F.P. and Ruzzante,D.E. (2008) Genetic estimates of contemporary effective population size: what can they tell us about the importance of genetic stochasticity for wild population persistence?*Mol. Ecol.*, **17**, 3428–3447.
12. Ross,S., Munkhtsog,B. and Harris,S. (2010) Dietary composition, plasticity, and prey selection of Pallas's cats. *J. Mammal.*, **91**, 811–817.
13. Barclay,D., Smelansky,I., Nygren,E. and Antonevich,A. (2019) In: *Legal Status, Utilisation, Management and Conservation of Manul*, pp. 37–40.
14. Johnson,W.E., Eizirik,E., Pecon-Slattery,J., Murphy,W.J., Antunes,A., Teeling,E. and O'Brien,S.J. (2006) The late miocene radiation of modern felidae: a genetic assessment. *Science*, **311**, 73–77.
15. Li,G., Davis,B.W., Eizirik,E. and Murphy,W.J. (2015) Phylogenomic evidence for ancient hybridization in the genomes of living cats (Felidae). *Genome Res.*, **26**, 1–11.
16. Sakamoto,M. and Ruta,M. (2012) Convergence and divergence in the evolution of cat skulls: temporal and spatial patterns of morphological diversity. *PLoS One*, **7**, e39752.
17. Mohamed,M., Dang,N.T.-M., Ogyama,Y., Burlet,N., Mugat,B., Boulesteix,M., Mérel,V., Salces-Ortiz,J., Severac,D. *et al.* (2020) A transposon story: from TE content to TE dynamic invasion of drosophila genomes using the single-molecule sequencing technology from Oxford nanopore. *Cells*, **9**, 1776.
18. Moss,E.L., Maghini,D.G. and Bhatt,A.S. (2020) Complete, closed bacterial genomes from microbiomes using nanopore sequencing. *Nat. Biotechnol.*, **38**, 701–707.
19. Ewing,A.D., Smits,N., Sanchez-Luque,F.J., Faivre,J., Brennan,P.M., Richardson,S.R., Cheetham,S.W. and Faulkner,G.J. (2020) Nanopore sequencing enables comprehensive transposable element epigenomic profiling. *Mol. Cell*, **80**, 915–928.
20. Razin,A. and Cedar,H. (1991) DNA methylation and gene expression. *Microbiol. Rev.*, **55**, 451–458.
21. Tate,P.H. and Bird,A.P. (1993) Effects of DNA methylation on DNA-binding proteins and gene expression. *Curr. Opin. Genet. Dev.*, **3**, 226–231.
22. Greenberg,M.V.C. and Bourc'his,D. (2019) The diverse roles of DNA methylation in mammalian development and disease. *Nat. Rev. Mol. Cell Biol.*, **20**, 590–607.
23. Zemach,A., McDaniel,I.E., Silva,P. and Zilberman,D. (2010) Genome-wide evolutionary analysis of eukaryotic DNA methylation. *Science*, **328**, 916–919.
24. Doskočil,J. and Šorm,F. (1962) Distribution of 5-methylcytosine in pyrimidine sequences of deoxyribonucleic acids. *Biochim. Biophys. Acta*, **55**, 953–959.
25. Riggs,A.D. (1975) X inactivation, differentiation, and DNA methylation. *Cytogenet. Genome Res.*, **14**, 9–25.
26. Cooper,D.N. and Krawczak,M. (1989) Cytosine methylation and the fate of CpG dinucleotides in vertebrate genomes. *Hum. Genet.*, **83**, 181–188.
27. Shafin,K., Pesout,T., Chang,P.-C., Nattestad,M., Kolesnikov,A., Goel,S., Baid,G., Kolmogorov,M., Eizenga,J.M., Miga,K.H. *et al.* (2021) Haplotype-aware variant calling with

PEPPER-Margin-DeepVariant enables high accuracy in nanopore long-reads. *Nat. Methods*, **18**, 1322–1332.
28. Battaglia,S., Dong,K., Wu,J., Chen,Z., Najm,F.J., Zhang,Y., Moore,M.M., Hecht,V., Shoresh,N. and Bernstein,B.E. (2022) Long-range phasing of dynamic, tissue-specific and allele-specific regulatory elements. *Nat. Genet.*, **54**, 1504–1513.
29. Akbari,V., Garant,J.-M., O'Neill,K., Pandoh,P., Moore,R., Marra,M.A., Hirst,M. and Jones,S.J. (2022) Genome-wide detection of imprinted differentially methylated regions using nanopore sequencing. *Elife*, **11**, e77898.
30. Rhie,A., McCarthy,S.A., Fedrigo,O., Damas,J. and Formenti,G. (2021) Towards complete and error-free genome assemblies of all vertebrate species. *Nature*, **592**, 737–746.
31. Kolmogorov,M., Yuan,J., Lin,Y. and Pevzner,P.A. (2019) Assembly of long, error-prone reads using repeat graphs. *Nat. Biotechnol.*, **37**, 540–546.
32. Shafin,K., Pesout,T., Lorig-Roach,R., Haukness,M., Olsen,H.E., Bosworth,C., Armstrong,J., Tigyi,K., Maurer,N., Koren,S. *et al.* (2020) Nanopore sequencing and the Shasta toolkit enable efficient de novo assembly of eleven human genomes. *Nat. Biotechnol.*, **38**, 1044–1053.
33. Vaser,R. and Šikić,M. (2021) Time- and memory-efficient genome assembly with Raven. *Nat. Comput. Sci.*, **1**, 332–336.
34. Vaser,R., Sović,I., Nagarajan,N. and Šikić,M. (2017) Fast and accurate de novo genome assembly from long uncorrected reads. *Genome Res.*, **27**, 737–746.
35. Hu,J., Fan,J., Sun,Z. and Liu,S. (2019) NextPolish: a fast and efficient genome polishing tool for long-read assembly. *Bioinformatics*, **36**, 2253–2255.
36. Manni,M., Berkeley,M.R., Seppey,M. and Zdobnov,E.M. (2021) BUSCO: assessing genomic data quality and beyond. *Curr. Protoc.*, **1**, e323.
37. Manni,M., Berkeley,M.R., Seppey,M., Simão,F.A. and Zdobnov,E.M. (2021) BUSCO update: novel and streamlined workflows along with broader and deeper phylogenetic coverage for scoring of eukaryotic, prokaryotic, and viral genomes. *Mol. Biol. Evol.*, **38**, 4647–4654.
38. Solares,E.A., Chakraborty,M., Miller,D.E., Kalsow,S., Hall,K., Perera,A.G., Emerson,J.J. and Hawley,R.S. (2018) Rapid low-cost assembly of the *Drosophila melanogaster* reference genome using low-coverage, long-read sequencing. *G3 (Bethesda)*, **8**, 3143–3154.
39. Solares,E.A., Chakraborty,M., Miller,D.E., Kalsow,S., Hall,K., Perera,A.G., Emerson,J.J. and Hawley,R.S. (2018) Rapid low-cost assembly of the *Drosophila melanogaster* reference genome using low-coverage, long-read sequencing. *G3 (Bethesda)*, **8**, 3143–3154.
40. Roach,M.J., Schmidt,S.A. and Borneman,A.R. (2018) Purge Haplotigs: allelic contig reassignment for third-gen diploid genome assemblies. *BMC Bioinf.*, **19**, 460.
41. Wood,D.E., Lu,J. and Langmead,B. (2019) Improved metagenomic analysis with Kraken 2. *Genome Biol.*, **20**, 257.
42. Breitwieser,F.P. and Salzberg,S.L. (2019) Pavian: interactive analysis of metagenomics data for microbiome studies and pathogen identification. *Bioinformatics*, **36**, 1303–1304.
43. Zhang,Z., Schwartz,S., Wagner,L. and Miller,W. (2000) A greedy algorithm for aligning DNA sequences. *J. Comput. Biol.*, **7**, 203–214.
44. Challis,R., Richards,E., Rajan,J., Cochrane,G. and Blaxter,M. (2020) BlobToolKit interactive quality assessment of genome assemblies. *G3 (Bethesda)*, **10**, 1361–1374.
45. Chen,Y., Zhang,Y., Wang,A.Y., Gao,M. and Chong,Z. (2021) Accurate long-read de novo assembly evaluation with Inspector. *Genome Biol.*, **22**, 312.
46. Rhie,A., Walenz,B.P., Koren,S. and Phillippy,A.M. (2020) Merqury: reference-free quality, completeness, and phasing assessment for genome assemblies. *Genome Biol.*, **21**, 245.
47. Storer,J., Hubley,R., Rosen,J., Wheeler,T.J. and Smit,A.F. (2021) The Dfam community resource of transposable element families, sequence models, and genome annotations. *Mobile DNA*, **12**, 2.
48. Keilwagen,J., Wenk,M., Erickson,J.L., Schattat,M.H., Grau,J. and Hartung,F. (2016) Using intron position conservation for homology-based gene prediction. *Nucleic Acids Res.*, **44**, e89–e89.
49. Keilwagen,J., Hartung,F., Paulini,M., Twardziok,S.O. and Grau,J. (2018) Combining RNA-seq data and homology-based gene prediction for plants, animals and fungi. *BMC Bioinf.*, **19**, 189.
50. Shumate,A. and Salzberg,S.L. (2021) Liftoff: accurate mapping of gene annotations. *Bioinformatics*, **37**, 1639–1643.
51. Martin,M., Ebert,P. and Marschall,T. (2023) Read-based phasing and analysis of phased variants with WhatsHap. In: Peters,B.A. and Drmanac,R. (eds). *Haplotyping. Methods in Molecular Biology*. Humana, NY, Vol. **2590**.
52. Danecek,P., Auton,A., Abecasis,G., Albers,C.A., Banks,E., DePristo,M.A., Handsaker,R.E., Lunter,G., Marth,G.T., Sherry,S.T. *et al.* (2011) The variant call format and VCFtools. *Bioinformatics*, **27**, 2156–2158.
53. Danecek,P., Bonfield,J.K., Liddle,J., Marshall,J. and Ohan,V. (2021) Twelve years of SAMtools and BCFtools, *GigaScience*, **10**, giab008.
54. Terhorst,J., Kamm,J.A. and Song,Y.S. (2016) Robust and scalable inference of population history from hundreds of unphased whole genomes. *Nat. Genet.*, **49**, 303–309.
55. Wu,H., Wang,C. and Wu,Z. (2012) A new shrinkage estimator for dispersion improves differential expression detection in RNA-seq data. *Biostatistics*, **14**, 232–243.
56. Feng,H., Conneely,K.N. and Wu,H. (2014) A Bayesian hierarchical model to detect differentially methylated loci from single nucleotide resolution sequencing data. *Nucleic Acids Res.*, **42**, e69–e69.
57. Wu,H., Xu,T., Feng,H., Chen,L., Li,B., Yao,B., Qin,Z., Jin,P. and Conneely,K.N. (2015) Detection of differentially methylated regions from whole-genome bisulfite sequencing data without replicates. *Nucleic Acids Res.*, **43**, 141.
58. Park,Y. and Wu,H. (2016) Differential methylation analysis for BS-seq data under general experimental design. *Bioinformatics*, **32**, 1446–1453.
59. Quinlan,A.R. and Hall,I.M. (2010) BEDTools: a flexible suite of utilities for comparing genomic features. *Bioinformatics*, **26**, 841–842.
60. Quinlan,A.R. (2014) BEDTools: the Swiss-Army tool for genome feature analysis. *Curr Protoc Bioinform.*, **47**, 11.12.1–11.12.34.
61. Cheetham,S.W., Kindlova,M. and Ewing,A.D. (2022) Methylartist: tools for visualizing modified bases from nanopore sequence data. *Bioinformatics*, **38**, 3109–3112.
62. Lin,J.-H., Chen,L.-C., Yu,S.-C. and Huang,Y.-T. (2022) LongPhase: an ultra-fast chromosome-scale phasing algorithm for small and large variants. *Bioinformatics*, **38**, 1816–1822.
63. Buels,R., Yao,E., Diesh,C.M., Hayes,R.D. and Munoz-Torres,M. (2016) JBrowse: a dynamic web platform for genome visualization and analysis. *Genome Biol.*, **17**, 66.
64. Lopez,J.V., Cevario,S. and O'Brien,S.J. (1996) Complete nucleotide sequences of the domestic cat (Felis catus) mitochondrial genome and a transposed mtDNA tandem repeat (Numt) in the nuclear genome. *Genomics*, **33**, 229–246.
65. Li,H. (2018) Minimap2: pairwise alignment for nucleotide sequences. *Bioinformatics*, **34**, 3094–3100.
66. Wanner,N., Larsen,P.A., McLain,A. and Faulk,C. (2021) The mitochondrial genome and Epigenome of the Golden lion Tamarin from fecal DNA using Nanopore adaptive sequencing. *BMC Genom.*, **22**, 726.
67. Edgar,R.C. (2004) MUSCLE: multiple sequence alignment with high accuracy and high throughput. *Nucleic Acids Res.*, **32**, 1792–1797.
68. Nguyen,L.-T., Schmidt,H.A., von Haeseler,A. and Minh,B.Q. (2014) IQ-TREE: a fast and effective stochastic algorithm for estimating maximum-likelihood phylogenies. *Mol. Biol. Evol.*, **32**, 268–274.
69. Alonge,M., Lebeigle,L., Kirsche,M., Aganezov,S., Wang,X., Lippman,Z.B., Schatz,M.C. and Soyk,S. (2021) Automated assembly scaffolding elevates a new tomato system for high-throughput genome editing. *Genome Biol*, **23**, 135.
70. Marçais,G., Delcher,A.L., Phillippy,A.M., Coston,R., Salzberg,S.L. and Zimin,A. (2018) MUMmer4: a fast and versatile genome alignment system. *PLoS Comput. Biol.*, **14**, e1005944.
71. Pontius,J.U., Mullikin,J.C., Smith,D.R., Lindblad-Toh,K., Gnerre,S., Clamp,M., Chang,J., Stephens,R., Neelam,B., Volfovsky,N. *et al.* (2007) Initial sequence and comparative analysis of the cat genome. *Genome Res.*, **17**, 1675–1689.
72. Buckley,R.M., Davis,B.W., Brashear,W.A., Farias,F.H.G., Kuroki,K., Graves,T., Hillier,L.W., Kremitzki,M., Li,G., Middleton,R.P. *et al.* (2020) A new domestic cat genome assembly based on long sequence reads empowers feline genomic medicine and identifies a novel gene for dwarfism. *PLoS Genet.*, **16**, e1008926.

73. Brashear,W.A., Bredemeyer,K.R. and Murphy,W.J. (2021) Genomic architecture constrained placental mammal X Chromosome evolution. *Genome Res.*, **31**, 1353–1365.
74. Burger,P.A., Steinborn,R., Walzer,C., Petit,T., Mueller,M. and Schwarzenberger,F. (2004) Analysis of the mitochondrial genome of cheetahs (Acinonyx jubatus) with neurodegenerative disease. *Gene*, **338**, 111–119.
75. Prost,S., Machado,A.P., Zumbroich,J., Preier,L., Mahtani-Williams,S., Meissner,R., Guschanski,K., Brealey,J.C., Fernandes,C.R., Vercammen,P. *et al.* (2022) Genomic analyses show extremely perilous conservation status of African and Asiatic cheetahs (*Acinonyx jubatus*). *Mol. Ecol.*, **31**, 4208–4223.
76. Bredemeyer,K.R., Seabury,C.M., Stickney,M.J., McCarrey,J.R., vonHoldt,B.M. and Murphy,W.J. (2021) Rapid macrosatellite evolution promotes X-linked hybrid male sterility in a feline interspecies cross. *Mol. Biol. Evol.*, **38**, 5588–5609.
77. Rhie,A., McCarthy,S.A., Fedrigo,O., Damas,J., Formenti,G., Koren,S., Uliano-Silva,M., Chow,W., Fungtammasan,A., Kim,J. *et al.* (2021) Towards complete and error-free genome assemblies of all vertebrate species. *Nature*, **592**, 737–746.
78. Abascal,F., Corvelo,A., Cruz,F., Villanueva-Cañas,J.L. and Vlasova,A. (2016) Extreme genomic erosion after recurrent demographic bottlenecks in the highly endangered Iberian lynx. *Genome Biol.*, **17**, 251.
79. Lei,W., XiaoBing,W., Zhu,L. and Jiang,Z. (2011) Mitogenomic analysis of the genus Panthera. *Sci. China Life Sci.*, **54**, 917–930.
80. Bredemeyer,K.R., Harris,A.J., Li,G., Zhao,L., Foley,N.M., Roelke-Parker,M., O'Brien,S.J., Lyons,L.A., Warren,W.C. and Murphy,W.J. (2020) Ultracontinuous single haplotype genome assemblies for the domestic cat (*Felis catus*) and asian leopard cat (*Prionailurus bengalensis*). *J. Hered.*, **112**, 165–173.
81. Tamazian,G., Dobrynin,P., Zhuk,A., Zhernakova,D.V., Perelman,P.L., Serdyukova,N.A., Graphodatsky,A.S., Komissarov,A., Kliver,S., Cherkasov,N. *et al.* (2021) Draft *de novo* genome assembly of the elusive jaguarundi, *Puma yagouaroundi*. *J. Hered.*, **112**, 540–548.
82. Faulk,C. (2023) *De novo* sequencing, diploid assembly, and annotation of the black carpenter ant, *Camponotus pennsylvanicus*, and its symbionts by one person for $1000, using nanopore sequencing. *Nucleic Acids Res.*, **51**, 17–28.
83. Armstrong,E.E., Taylor,R.W., Miller,D.E., Kaelin,C.B., Barsh,G.S., Hadly,E.A. and Petrov,D. (2020) Long live the king: chromosome-level assembly of the lion (*Panthera leo*) using linked-read, Hi-C, and long-read data. *BMC Biol.*, **18**, 3.
84. Schrader,L. and Schmitz,J. (2018) The impact of transposable elements in adaptive evolution. *Mol. Ecol.*, **28**, 1537–1549.
85. Böhne,A., Brunet,F., Galiana-Arnoux,D., Schultheis,C. and Volff,J.-N. (2008) Transposable elements as drivers of genomic and biological diversity in vertebrates. *Chromosome Res.*, **16**, 203–215.
86. Platt,R.N., Vandewege,M.W. and Ray,D.A. (2018) Mammalian transposable elements and their impacts on genome evolution. *Chromosome Res.*, **26**, 25–43.
87. Meredith,R.W., Janecka,J.E., Gatesy,J., Ryder,O.A., Fisher,C.A., Teeling,E.C., Goodbla,A., Eizirik,E., Simao,T.L.L., Stadler,T. *et al.* (2011) Impacts of the cretaceous terrestrial revolution and KPg extinction on mammal diversification. *Science*, **334**, 521–524.
88. Ehrlich,M., Gama-Sosa,M.A., Huang,L.-H., Midgett,R.M., Kuo,K.C., McCune,R.A. and Gehrke,C. (1982) Amount and distribution of 5-methylcytosine in human DNA from different types of tissues or cells. *Nucleic Acids Res.*, **10**, 2709–2721.
89. Bastepe,M., Fröhlich,L.F., Linglart,A., Abu-Zahra,H.S., Tojo,K., Ward,L.M. and Jüppner,H. (2004) Deletion of the NESP55 differentially methylated region causes loss of maternal GNAS imprints and pseudohypoparathyroidism type Ib. *Nat. Genet.*, **37**, 25–27.
90. Zaitoun,I. and Khatib,H. (2006) Assessment of genomic imprinting of *SLC38A4*, *NNAT*, *NAP1L5*, and *H19* in cattle. *BMC Genet.*, **7**, 49.
91. Brabazon,D.C., Callanan,J.J. and Nolan,C.M. (2021) Imprinting of canine *IGF2* and *H19*. *Anim. Genet.*, **53**, 108–118.
92. Eßinger,C., Karch,S., Moog,U., Fekete,G., Lengyel,A., Pinti,E., Eggermann,T. and Begemann,M. (2020) Frequency of *KCNQ1* variants causing loss of methylation of Imprinting Centre 2 in Beckwith-Wiedemann syndrome. *Clin Epigenet*, **12**, 63.
93. Li,X., Song,N., Wang,D., Han,X., Lv,Q., Ouyang,H. and Li,Z. (2015) Isoform-specific imprinting of the MEST gene in porcine parthenogenetic fetuses. *Gene*, **558**, 287–290.
94. Kobayashi,H., Yamada,K., Morita,S., Hiura,H., Fukuda,A., Kagami,M., Ogata,T., Hata,K., Sotomaru,Y. and Kono,T. (2009) Identification of the mouse paternally expressed imprinted gene Zdbf2 on chromosome 1 and its imprinted human homolog ZDBF2 on chromosome 2. *Genomics*, **93**, 461–472.
95. Kobayashi,H., Yanagisawa,E., Sakashita,A., Sugawara,N., Kumakura,S., Ogawa,H., Akutsu,H., Hata,K., Nakabayashi,K. and Kono,T. (2013) Epigenetic and transcriptional features of the novel human imprinted lncRNA*GPR1AS*suggest it is a functional ortholog to mouse*Zdbf2linc*. *Epigenetics*, **8**, 635–645.
96. Iwata,K., Kawarabayashi,K., Yoshizaki,K., Tian,T., Saito,K., Sugimoto,A., Kurogoushi,R., Yamada,A., Yamamoto,A., Kudo,Y. *et al.* (2021) von Willebrand factor D and EGF domains regulate ameloblast differentiation and enamel formation. *J. Cell. Physiol.*, **237**, 1964–1979.
97. Kobayashi,H., Yanagisawa,E., Sakashita,A., Sugawara,N., Kumakura,S., Ogawa,H., Akutsu,H., Hata,K., Nakabayashi,K. and Kono,T. (2013) Epigenetic and transcriptional features of the novel human imprinted lncRNA*GPR1AS*suggest it is a functional ortholog to mouse*Zdbf2linc*. *Epigenetics*, **8**, 635–645.
98. Xu,Y., Liu,J., Jiang,E., Xu,Y., Ning,F., Du,Z. and Bai,X. (2019) The complete mitochondrial genome of Pallas's cat (*Otocolobus manul*). *Mitochondrial DNA B*, **4**, 658–659.
99. Paez,S., Kraus,R.H.S., Shapiro,B., Thomas,M., Gilbert,P., Jarvis,E.D. and Vertebrate Genomes Project Conservation GroupVertebrate Genomes Project Conservation Group, Al-Ajli,FO, Ceballos,G, Crawford,AJ and Fedrigo,O. (2022) Reference genomes for conservation. *Science*, **377**, 364–366.
100. Morin,P.A., Archer,F.I., Avila,C.D., Balacco,J.R., Bukhman,Y.V., Chow,W., Fedrigo,O., Formenti,G., Fronczek,J.A., Fungtammasan,A. *et al.* (2020) Reference genome and demographic history of the most endangered marine mammal, the vaquita. *Mol. Ecol. Resour.*, **21**, 1008–1020.
101. Murigneux,V., Rai,S.K., Furtado,A., Bruxner,T.J.C., Tian,W., Harliwong,I., Wei,H., Yang,B., Ye,Q., Anderson,E. *et al.* (2020) Comparison of long-read methods for sequencing and assembly of a plant genome. *Gigascience*, **9**, 12.
102. Wick,R.R. and Holt,K.E. (2019) Benchmarking of long-read assemblers for prokaryote whole genome sequencing. *F1000Res*, **8**, 2138.
103. Chen,Z., Erickson,D.L. and Meng,J. (2020) Benchmarking long-read assemblers for genomic analyses of bacterial pathogens using Oxford Nanopore Sequencing. *Int. J. Mol. Sci.*, **21**, 9161.
104. Hotaling,S., Kelley,J.L. and Frandsen,P.B. (2021) Toward a genome sequence for every animal: where are we now?. *Proc. Nat. Acad. Sci. U.S.A.*, **118**, e2109019118.
105. Bhat,A., Ghatage,T., Bhan,S., Lahane,G.P., Dhar,A., Kumar,R., Pandita,R.K., Bhat,K.M., Ramos,K.S. and Pandita,T.K. (2022) Role of transposable elements in genome stability: implications for health and disease. *Int. J. Mol. Sci.*, **23**, 7802.
106. Lavialle,C., Cornelis,G., Dupressoir,A., Esnault,C., Heidmann,O., Vernochet,C. and Heidmann,T. (2013) Paleovirology of '*syncytins*', retroviral *env* genes exapted for a role in placentation. *Philos. Trans. R Soc. Lond. B Biol. Sci.*, **368**, 20120507.
107. Stoye,J.P. (2012) Studies of endogenous retroviruses reveal a continuing evolutionary saga. *Nat. Rev. Microbiol.*, **10**, 395–406.
108. Chiu,E.S. and VandeWoude,S. (2020) Presence of endogenous viral elements negatively correlates with feline leukemia virus susceptibility in Puma and domestic cat cells. *J. Virol.*, **94**, e01274-20.
109. Walters-Conte,K.B., Johnson,D.L.E., Allard,M.W. and Pecon-Slattery,J. (2011) Carnivore-specific SINEs (Can-SINEs): distribution, evolution, and genomic impact. *J. Hered.*, **102**, S2–S10.
110. Wiedmer,M., Oevermann,A., Borer-Germann,S.E., Gorgas,D., Shelton,G.D., Drögemüller,M., Jagannathan,V., Henke,D. and Leeb,T. (2016) A *RAB3GAP1* SINE Insertion in Alaskan Huskies with Polyneuropathy, Ocular Abnormalities, and Neuronal Vacuolation (POANV) Resembling Human Warburg Micro Syndrome 1 (WARBM1). *G3 (Bethesda)*, **6**, 255–262.
111. Goldstein,O., Kukekova,A.V., Aguirre,G.D. and Acland,G.M. (2010) Exonic SINE insertion in STK38L causes canine early retinal degeneration (erd). *Genomics*, **96**, 362–368.

112. Pelé,M., Tiret,L., Kessler,J.-L., Blot,S. and Panthier,J.-J. (2005) SINE exonic insertion in the PTPLA gene leads to multiple splicing defects and segregates with the autosomal recessive centronuclear myopathy in dogs. *Hum. Mol. Genet.*, **14**, 1417–1427.
113. Wang,W. and Kirkness,E.F. (2005) Short interspersed elements (SINEs) are a major source of canine genomic diversity. *Genome Res.*, **15**, 1798–1808.
114. Clark,L.A., Wahl,J.M., Rees,C.A. and Murphy,K.E. (2006) Retrotransposon insertion in *SILV* is responsible for merle patterning of the domestic dog. *Proc. Natl. Acad. Sci. U.S.A.*, **103**, 1376–1381.
115. Murphy,S.C., Evans,J.M., Tsai,K.L. and Clark,L.A. (2018) Length variations within the Merle retrotransposon of canine PMEL: correlating genotype with phenotype. *Mobile DNA*, **9**, 26.
116. Okada,M., Yoshikawa,R., Shojima,T., Baba,K. and Miyazawa,T. (2011) Susceptibility and production of a feline endogenous retrovirus (RD-114 virus) in various feline cell lines. *Virus Res.*, **155**, 268–273.
117. Okabe,H., Gilden,R.V. and Hatanaka,M. (1973) RD 114 virus-specific sequences in feline cellular RNA: detection and characterization. *J. Virol.*, **12**, 984–994.
118. Yoshikawa,R., Shimode,S., Sakaguchi,S. and Miyazawa,T. (2013) Contamination of live attenuated vaccines with an infectious feline endogenous retrovirus (RD-114 virus). *Arch. Virol*, **159**, 399–404.
119. Yasir,M., Turner,A.K., Lott,M., Rudder,S., Baker,D., Bastkowski,S., Page,A.J., Webber,M.A. and Charles,I.G. (2022) Long-read sequencing for identification of insertion sites in large transposon mutant libraries. *Sci. Rep.*, **12**, 3546.
120. Logsdon,G.A., Vollger,M.R. and Eichler,E.E. (2020) Long-read human genome sequencing and its applications. *Nat. Rev. Genet.*, **21**, 597–614.
121. Miga,K.H., Koren,S., Rhie,A., Vollger,M.R., Gershman,A., Bzikadze,A., Brooks,S., Howe,E., Porubsky,D., Logsdon,G.A. *et al.* (2020) Telomere-to-telomere assembly of a complete human X chromosome. *Nature*, **585**, 79–84.
122. Raj,K., Szladovits,B., Haghani,A., Zoller,J.A., Li,C.Z., Black,P., Maddox,D., Robeck,T.R. and Horvath,S. (2021) Epigenetic clock and methylation studies in cats. *GeroScience*, **43**, 2363–2378.
123. Horvath,S. (2013) DNA methylation age of human tissues and cell types. *Genome Biol.*, **14**, R115.
124. Ekström,T.J. (1994) Parental Imprinting and the *IGF2* gene. *Horm. Res.*, **42**, 176–181.
125. Tucci,V., Isles,A.R., Kelsey,G., Ferguson-Smith,A.C., Tucci,V., Bartolomei,M.S., Benvenisty,N., Bourc'his,D., Charalambous,M., Dulac,C. *et al.* (2019) Genomic imprinting and physiological processes in mammals. *Cell*, **176**, 952–965.
126. Bartolomei,M.S., Zemel,S. and Tilghman,S.M. (1991) Parental imprinting of the mouse H19 gene. *Nature*, **351**, 153–155.
127. Jima,D.D., Skaar,D.A., Planchart,A., Motsinger-Reif,A., Cevik,S.E., Park,S.S., Cowley,M., Wright,F., House,J., Liu,A. *et al.* (2022) Genomic map of candidate human imprint control regions: the imprintome. *Epigenetics*, **17**, 1920–1943.
128. Kanduri,C., Fitzpatrick,G., Mukhopadhyay,R., Kanduri,M., Lobanenkov,V., Higgins,M. and Ohlsson,R. (2002) A differentially methylated imprinting control region within the Kcnq1 locus harbors a methylation-sensitive chromatin insulator. *J. Biol. Chem.*, **277**, 18106–18110.
129. O'Sullivan,F.M., Murphy,S.K., Simel,L.R., McCann,A., Callanan,J.J. and Nolan,C.M. (2007) Imprinted expression of the canine IGF2R, in the absence of an anti-sense transcript or promoter methylation. *Evol. Dev.*, **9**, 579–589.
130. Nolan,C., O'Sullivan,F., Brabazon,D. and Callanan,J. (2009) Genomic Imprinting in*Canis familiaris*. *Reprod Domestic Anim.*, **44**, 16–21.
131. Killian,J.K. (2001) Divergent evolution in M6P/IGF2R imprinting from the jurassic to the quaternary. *Hum. Mol. Genet.*, **10**, 1721–1728.
132. Leigh,N.D., Sessa,S., Dragalzew,A.C., Payzin-Dogru,D., Sousa,J.F., Aggouras,A.N., Johnson,K., Dunlap,G.S., Haas,B.J., Levin,M. *et al.* (2020) von Willebrand factor D and EGF domains is an evolutionarily conserved and required feature of blastemas capable of multitissue appendage regeneration. *Evol. Dev.*, **22**, 297–311.
133. MacArthur,D.G., Balasubramanian,S., Frankish,A., Huang,N., Morris,J., Walter,K., Jostins,L., Habegger,L., Pickrell,J.K., Montgomery,S.B. *et al.* (2012) A systematic survey of loss-of-function variants in human protein-coding genes. *Science*, **335**, 823–828.
134. Tucci,V., Isles,A.R., Kelsey,G., Ferguson-Smith,A.C., Tucci,V., Bartolomei,M.S., Benvenisty,N., Bourc'his,D., Charalambous,M., Dulac,C. *et al.* (2019) Genomic imprinting and physiological processes in mammals. *Cell*, **176**, 952–965.
135. Henry,P., Miquelle,D., Sugimoto,T., McCullough,D.R., Caccone,A. and Russello,M.A. (2009) *In situ*population structure and*ex situ*representation of the endangered Amur tiger. *Mol. Ecol.*, **18**, 3173–3184.
136. Cho,Y., Hu,L., Hou,H., Lee,H. and Xu,J. (2013) The tiger genome and comparative analysis with lion and snow leopard genomes. *Nat. Commun.*, **4**, 2433.
137. Liao,W. and Reed,D.H. (2009) Inbreeding-environment interactions increase extinction risk. *Animal Conserv.*, **12**, 54–61.
138. Ning,Y., Kostyria,A.V., Ma,J., Chayka,M.I., Guskov,V.Y., Qi,J., Sheremetyeva,I.N., Wang,M. and Jiang,G. (2019) Dispersal of Amur tiger from spatial distribution and genetics within the eastern Changbai mountain of China. *Ecol. Evol.*, **9**, 2415–2424.
139. Howell,L.G., Frankham,R., Rodger,J.C., Witt,R.R., Clulow,S., Upton,R.M.O. and Clulow,J. (2021) Integrating biobanking minimises inbreeding and produces significant cost benefits for a threatened frog captive breeding programme. *Conserv. Lett.*, **14**, e12776.
140. Bernt,M., Braband,A., Schierwater,B. and Stadler,P.F. (2013) Genetic aspects of mitochondrial genome evolution. *Mol. Phylogenet. Evol.*, **69**, 328–338.
141. Birky,C.W. (2008) Uniparental inheritance of organelle genes. *Curr. Biol.*, **18**, R692–R695.
142. Goremykin,V.V., Salamini,F., Velasco,R. and Viola,R. (2008) Mitochondrial DNA of vitis vinifera and the issue of rampant horizontal gene transfer. *Mol. Biol. Evol.*, **26**, 99–110.
143. Folk,R.A., Mandel,J.R. and Freudenstein,J.V. (2016) Ancestral gene flow and parallel organellar genome capture result in extreme phylogenomic discord in a lineage of angiosperms. *Syst. Biol.*, **66**, 320–337.
144. Yu,H., Xing,Y.-T., Meng,H., He,B., Li,W.-J., Qi,X.-Z., Zhao,J.-Y., Zhuang,Y., Xu,X. and Luo,S. (2021) Genomic evidence for the Chinese mountain cat as a wildcat conspecific (*Felis silvestris bieti*) and its introgression to domestic cats. *Sci. Adv.*, **7**, 26.
145. Le Roux,J.J., Foxcroft,L.C., Herbst,M. and MacFadyen,S. (2014) Genetic analysis shows low levels of hybridization between A frican wildcats (*Felis silvestris lybica*) and domestic cats (*F. s. catus*) in S outh A frica. *Ecol. Evol.*, **5**, 288–299.
146. Pierpaoli,M., Birò,Z.S., Herrmann,M., Hupe,K., Fernandes,M., Ragni,B., Szemethy,L. and Randi,E. (2003) Genetic distinction of wildcat (*Felis silvestris*) populations in Europe, and hybridization with domestic cats in Hungary. *Mol. Ecol.*, **12**, 2585–2598.
147. Asase,A., Mzumara-Gawa,T.I., Owino,J.O., Peterson,A.T. and Saupe,E. (2022) Replacing "parachute science" with "global science" in ecology and conservation biology. *Conserv Sci Pract*, **4**, e517.
148. Stefanoudis,P.V., Licuanan,W.Y., Morrison,T.H., Talma,S., Veitayaki,J. and Woodall,L.C. (2021) Turning the tide of parachute science. *Curr. Biol.*, **31**, R184–R185.
149. Li,F.-W. (2021) Decolonizing botanical genomics. *Nat. Plants*, **7**, 1542–1543.